Dynamic magnetic response of a ferrofluid in a static uniform magnetic field

Dynamic magnetic response of a ferrofluid in a static uniform magnetic field

Timur M. Batrudinov, Yuliya E. Nekhoroshkova, Egor I. Paramonov,
Vladimir S. Zverev, Ekaterina A. Elfimova, and Alexey O. Ivanov
Department of Theoretical and Mathematical Physics,
Institute of Natural Sciences and Mathematics, Ural Federal University,
51 Lenin Avenue, Ekaterinburg, 620000, Russia

Philip J. Camp*
School of Chemistry, University of Edinburgh,
David Brewster Road, Edinburgh EH9 3FJ, Scotland and
Department of Theoretical and Mathematical Physics,
Institute of Natural Sciences and Mathematics, Ural Federal University,
51 Lenin Avenue, Ekaterinburg, 620000, Russia

(Dated: 18 October 2018)

Abstract

A theory for the frequency-dependent magnetic susceptibility of a ferrofluid in a static uniform magnetic field is developed, including the dipolar interactions between the constituent particles. Interactions are included within the framework of modified mean-field theory. Predictions are given for the linear responses of the magnetization to a probing ac field both parallel and perpendicular to the static field, and are tested against results from Brownian dynamics simulations. The effects of particle concentration and dipolar coupling constant on the field-dependent static susceptibilities and the frequency dispersions are shown to be substantial, which justifies taking proper account of the interactions between particles. The theory is reliable provided that the volume concentration and dipolar coupling constant are not too large, and within the range of values for real ferrofluids.

* Corresponding author: philip.camp@ed.ac.uk

I. INTRODUCTION

One of the defining characteristics of magnetic fluids is the ability to control the physical properties of the material by the application of uniform and non-uniform magnetic fields. The interaction between the constituent magnetic particles and the applied field can cause dramatic changes in the structural organization of the particles within the non-magnetic carrier fluid, and this results in substantial changes to the optical and magnetic properties, the dynamical quantities such as viscosity, and the thermodynamic functions [1, 2]. A particularly important example of such a system is a ferrofluid, in which the magnetic nanoparticles – roughly 10 nm in diameter – are ferromagnetic, meaning that the magnetic dipole moment reorients mainly due to Brownian rotational motion of the particle as a whole. Smaller nanoparticles exhibit superparamagnetism, in which the magnetic dipole moment flips through the Néel mechanism [2].

Ferrofluids have been studied extensively, both experimentally and theoretically, and the literature is vast. From the theoretical point of view, the static and thermodynamic properties of ferrofluids can be predicted quite reliably; for a recent review, see Ref. 3. In this work, the focus is on the response of a ferrofluid to a weak ac magnetic field, while the system is magnetized by a static magnetic field. The linear response to the probing ac field is characterized by the frequency-dependent susceptibility spectrum. The susceptibility spectrum is an important physical property, because its imaginary (out-of-phase) part controls the power dissipation in the ferrofluid [4]. The dissipation of heat can be exploited in the medical treatment of diseased tissue by localized heating (hyperthermia) [5–9], and it is important for developing new applications to understand how material parameters control the power loss [10–12].

In the absence of dipole-dipole interactions, and in the presence of only the probing ac field, the mathematical problem of computing the susceptibility spectrum is rather straightforward. The general approach is based on solving the Fokker-Planck-Brown equation for the one-particle orientational distribution function [13, 14]. The results are familiar as the Debye theory of polar media [15, 16], which gives simple closed-form expressions for the susceptibility spectrum in terms of the Brownian rotation time and the static (Langevin) susceptibility. Many attempts have been made to include the effects of dipole-dipole interactions [17–22]. In recent work by some of the current authors, an approach based on the

so-called modified mean-field theory [23] was developed to enable interactions to be included in a systematic way, based on classical statistical mechanics [24, 25]. This is a perturbation theory, and so far, only the leading-order corrections have been incorporated in the dynamical case. Tests against Brownian dynamics (BD) simulations have been used to determine the range of applicability of the theory, in terms of material parameters such as particle concentration and the strength of the dipole-dipole interactions [26–28].

In the presence of a static field, the problem gets rather more complicated [29, 30]. Firstly, there are two susceptibility spectra, corresponding to the probing ac field being either parallel or perpendicular to the static field. Secondly, the mathematical analysis of the dynamics leads to the identification of a spectrum of timescales, even though in practice the longest timescale may be sufficient. In a lot of experimental work, the theoretical expressions for non-interacting systems have been used to analyze measured properties [31–33]. So far, there is no theory for the dynamics of a system in a static field that includes the effects of dipole-dipole interactions. The aim of the current work is to fill that gap using the modified mean-field approach, and to test the predictions against numerical results from BD simulations. An outline of the theoretical framework for non-interacting systems has already been published [34], and this paves the way for including interactions.

The rest of this article is organized as follows. The basic microscopic model and some elementary properties of non-interacting systems are outlined in Section II A. The theory is detailed in Sections II B and II C, organized in terms of the probing ac field being, respectively, parallel and perpendicular to the static field. The technical details in the two cases are different, but for clarity, the derivations are organized in the same way, as far as possible. Section II D describes the BD simulations. The results are presented in Section III, and Section IV concludes the article.

II. MODEL, THEORY, AND SIMULATIONS

A. Model and basic properties

The system is modeled as a suspension of N spherical magnetic particles with equal diameters σ and dipole moments μ, immersed in a structureless fluid at temperature T with viscosity η and total volume V. The short-range interactions can be either of the

hard-sphere form or, more conveniently for BD simulations, given by the Weeks-Chandler-Andersen (WCA) potential

$$u_{ij}^{\mathrm{s}} = \begin{cases} 4\epsilon \left[\left(\dfrac{\sigma}{r_{ij}} \right)^{12} - \left(\dfrac{\sigma}{r_{ij}} \right)^{6} \right] + \epsilon & r_{ij} \leq r_{\min} \\ 0 & r_{ij} > r_{\min} \end{cases} \tag{1}$$

where ϵ is the Lennard-Jones energy parameter, r_{ij} is the separation between particles i and j, and $r_{\min} = 2^{1/6}\sigma$ is the position of the minimum in the Lennard-Jones potential. The dipole-dipole interaction potential is

$$u_{ij}^{\mathrm{d}} = \frac{\mu_0}{4\pi} \left[\frac{(\boldsymbol{\mu}_i \cdot \boldsymbol{\mu}_j)}{r_{ij}^3} - \frac{3(\boldsymbol{\mu}_i \cdot \boldsymbol{r}_{ij})(\boldsymbol{\mu}_j \cdot \boldsymbol{r}_{ij})}{r_{ij}^5} \right] \tag{2}$$

where μ_0 is the vacuum permeability, $\boldsymbol{\mu}_i = \mu(\sin\theta_i \cos\phi_i, \sin\theta_i \sin\phi_i, \cos\theta_i)$ is the dipole moment on particle i, and $\boldsymbol{r}_{ij} = \boldsymbol{r}_j - \boldsymbol{r}_i$ is the separation vector between particles i and j. The strength of the dipole-dipole interactions is characterized by the dipolar coupling constant

$$\lambda = \frac{\mu_0 \mu^2}{4\pi\sigma^3 k_{\mathrm{B}} T} \tag{3}$$

where k_{B} is Boltzmann's constant. A static external magnetic field of strength H_z is applied in the z direction. The Langevin parameter characterizing the strength of the dipole-field interaction $-\mu_0(\boldsymbol{\mu} \cdot \boldsymbol{H})$ is

$$\alpha_z = \frac{\mu_0 \mu H_z}{k_{\mathrm{B}} T}. \tag{4}$$

The potential energy of a single dipole, i, in units of the thermal energy $k_{\mathrm{B}}T$ is

$$\frac{U_i}{k_{\mathrm{B}}T} = \frac{1}{k_{\mathrm{B}}T} \sum_{j \neq i}^{N} \left(u_{ij}^{\mathrm{s}} + u_{ij}^{\mathrm{d}} \right) - \alpha_z \cos\theta_i. \tag{5}$$

For non-interacting particles, the magnetization curve is given by the simple Langevin law

$$M_z^{\mathrm{id}}(H_z) = \rho\mu L(\alpha_z) \tag{6}$$

where $\rho = N/V$ is the number concentration of particles in the system, and $L(t) = \coth t - t^{-1}$. The Langevin static susceptibility is

$$\chi_{\mathrm{L}} = \frac{\rho\mu_0\mu^2}{3k_{\mathrm{B}}T} = 8\varphi\lambda \tag{7}$$

where $\varphi = \pi\rho\sigma^3/6$ is the volume fraction. Elementary calculations give the field-dependent susceptibilities both perpendicular (xy) and parallel (z) to the applied static magnetic field.

$$\chi_{xy}^{\mathrm{id}}(0) = 3\chi_{\mathrm{L}}\left(\frac{\coth\alpha_z}{\alpha_z} - \frac{1}{\alpha_z^2}\right) = \frac{3\chi_{\mathrm{L}}L(\alpha_z)}{\alpha_z} \tag{8}$$

$$\chi_{z}^{\mathrm{id}}(0) = 3\chi_{\mathrm{L}}\left(1 - \coth^2\alpha_z + \frac{1}{\alpha_z^2}\right) = 3\chi_{\mathrm{L}}L_1(\alpha_z) \tag{9}$$

A function $L_1(t) = \mathrm{d}L/\mathrm{d}t$ is defined in Eq. (9). The dynamical properties are considered theoretically in the following two sections, and the frequency-dependent susceptibility of a ferrofluid in a static magnetic field will be determined, taking into account interactions between the constituent particles. For technical reasons, it is convenient to treat two different cases separately: first, the case where the probing ac field is parallel to the static field (Section II B); and second, the case where the probing ac field is perpendicular to the static field (Section II C). As far as possible, the same notation will be used in each section to highlight the similarities between the derivations, but the details will be different. In each case, results for non-interacting systems will be outlined first [34], and then the effects of interactions will be described.

B. Dynamical properties: the frequency-dependent susceptibility parallel to a static magnetic field

The ferrofluid is contained in a long, cylindrical tube oriented along the z axis. The magnetic field applied to the ferrofluid is of the form

$$\boldsymbol{H} = \left(0, 0, H_z + he^{i\omega t}\right) \tag{10}$$

where the probing ac field strength h is small. Note that the static field causes a net magnetization of the sample, and that the weak, time-dependent, probing field causes a perturbation to the magnetization, which is used only to define the frequency-dependent susceptibility within the linear-response regime. Because the applied and probing fields are parallel to the symmetry axis of the cylindrical container, there are no demagnetization effects. Due to the symmetry of the system, the orientation of each dipole need only be described with the polar angle θ. The probability distribution function of θ is denoted by $W(\theta, t)$, and is a solution of the Fokker-Planck equation

$$2\tau_{\mathrm{B}}\frac{\partial W}{\partial t} = \frac{1}{\sin\theta}\frac{\partial}{\partial\theta}\left[\sin\theta\left(\frac{\partial W}{\partial\theta} + \frac{W}{k_{\mathrm{B}}T}\frac{\partial U}{\partial\theta}\right)\right] \tag{11}$$

where U is the potential energy of a dipole. $\tau_{\rm B}$ is the Brownian rotational time, given by

$$\tau_{\rm B} = \frac{1}{2D_{\rm rot}} = \frac{\pi\eta\sigma^3}{2k_{\rm B}T} \tag{12}$$

where $D_{\rm rot}$ is the rotational diffusion coefficient. In previous work [29, 30], the dynamics of the magnetization parallel to the applied field were found to be controlled by a spectrum of relaxation times, the longest of which is

$$\tau_{\parallel} = \left[\frac{\alpha_z L_1(\alpha_z)}{L(\alpha_z)}\right]\tau_{\rm B} \tag{13}$$

which in small fields reduces to $\tau_{\parallel} = \left(1 - \frac{2}{15}\alpha_z^2\right)\tau_{\rm B}$. The imaginary part of the susceptibility spectrum would be expected to show a peak at a frequency $\Omega_{\parallel} \simeq \tau_{\parallel}^{-1}$, which increases with increasing field strength.

1. *Non-interacting particles*

In the absence of interparticle interactions – denoted the ideal (id) case – such as at low concentrations, the potential energy of a dipole in units of $k_{\rm B}T$ is simply

$$\frac{U}{k_{\rm B}T} = -\left(\alpha_z + \alpha e^{i\omega t}\right)\cos\theta \tag{14}$$

where the dipole label is omitted, and $\alpha = \mu_0\mu h/k_{\rm B}T$ is the Langevin parameter for the probing ac field in the z direction. Within the linear-response regime, where $\alpha \ll 1$, the solution of Eq. (11) can be expressed in the following form.

$$W^{\rm id}(\theta, t) = \left(\frac{\alpha_z}{\sinh\alpha_z}\right)e^{\alpha_z\cos\theta} + \alpha e^{i\omega t}\sum_{n=0}^{\infty} Z_n^{\rm id} P_n(\cos\theta) \tag{15}$$

The first term on the rhs is the unnormalized equilibrium Boltzmann distribution, and the second term is the perturbation introduced by the probing ac field. Inserting Eq. (15) in to Eq. (11), linearizing the equation to first order in α, and using the orthogonality of the Legendre polynomials P_n gives a recurrence relation for the coefficients $Z_n^{\rm id}$,

$$-Z_{n-1}^{\rm id}\left[\frac{\alpha_z n(n+1)}{2n-1}\right] + Z_n^{\rm id}\left[n(n+1) + 2i\omega\tau_{\rm B}\right] + Z_{n+1}^{\rm id}\left[\frac{\alpha_z n(n+1)}{2n+3}\right] = -\left(\frac{2n+1}{2}\right)F_n(\alpha_z) \tag{16}$$

with $Z_0^{\rm id} = 0$, and where

$$F_n(a) = \left(\frac{a}{\sinh a}\right)\int_{-1}^{1} P_n(x)\frac{\rm d}{{\rm d}x}\left[e^{ax}(1-x^2)\right]\ {\rm d}x. \tag{17}$$

Equation (16) shows that the coefficients depend on α_z and ω. Explicit expressions for $Z_n^{\rm id}$ can be determined by truncating the sum in Eq. (15) at some arbitrary order $n = k$, setting $Z_{n>k}^{\rm id} = 0$, and solving the set of k algebraic equations. Once $W^{\rm id}$ is determined, the magnetization is given by

$$\begin{aligned} M_z^{\rm id}(t) &= \frac{1}{2}\rho\mu \int_{-1}^{1} W^{\rm id}(\theta,t)\cos\theta \ {\rm d}\cos\theta \\ &= \frac{1}{2}\rho\mu \int_{-1}^{1} \left[\left(\frac{\alpha_z}{\sinh\alpha_z}\right) e^{\alpha_z x} + \alpha e^{i\omega t} Z_1^{\rm id} P_1(x)\right] x \ {\rm d}x \\ &= \rho\mu L(\alpha_z) + \chi_{\rm L} h e^{i\omega t} Z_1^{\rm id} \end{aligned} \tag{18}$$

where $Z_1^{\rm id}$ is the only coefficient that appears because $\int_{-1}^{1} x P_n(x) \ {\rm d}x = \frac{2}{3}$ for $n = 1$ and zero otherwise. The frequency-dependent susceptibility is

$$\chi_z^{\rm id}(\omega) = \frac{\partial M_z^{\rm id}}{\partial(he^{i\omega t})} = \chi_{\rm L} Z_1^{\rm id} \tag{19}$$

which shows that $Z_1^{\rm id}$ is the key coefficient, although it depends on higher-order coefficients through the recurrence relation in Eq. (16). In this work, Eq. (15) is truncated at $n = 5$, i.e., $Z_{n>5}^{\rm id} = 0$. The solution of the five algebraic equations is tedious, and the essential details are given in Appendix A; but it is stressed once again that all of the coefficients depend on both α_z and ω, and in particular, the first coefficient will be written $Z_1^{\rm id} = G(\alpha_z, \omega\tau_{\rm B})$, where G has the property that $G(0,0) = 1$. In the zero-frequency limit ($\omega\tau_{\rm B} \to 0$), the static susceptibility is given by

$$\chi_z^{\rm id}(0) = \chi_{\rm L} G(\alpha_z, 0) \tag{20}$$

$$G(\alpha_z, 0) = 3\left[\frac{L(\alpha_z)(\alpha_z^4 + 180\alpha_z^2 + 2475) - 6\alpha_z(3\alpha_z^2 + 110)}{\alpha_z(\alpha_z^4 + 60\alpha_z^2 + 495)}\right]. \tag{21}$$

This is an approximate equation arising from the truncation of Eq. (15), and a comparison between this and the exact formula in Eq. (9) will be made in Section III A. In the limit $\alpha_z \to 0$, $G(0,0) = 1$, and the correct Langevin initial susceptibility is obtained.

2. Interacting particles

Following earlier work [24], interactions between particles are described by an effective field acting on each particle. This is achieved within the framework of the first-order modified mean-field (MMF1) theory [23–25]. In brief, this approximation is based on the interaction

energy for dipole 1 in Eq. (5) being written

$$\frac{U_1}{k_\mathrm{B}T} = -\frac{\rho}{k_\mathrm{B}T}\left\langle W^\mathrm{id}(\theta_2,t)u_{12}^\mathrm{d}\Theta(r_{12}-\sigma)\right\rangle_2 - \alpha_z\cos\theta_1 \tag{22}$$

where Θ is the Heaviside function representing the impenetrability of particles 1 and 2. The angled brackets denote an integration over the position and orientation of particle 2:

$$\langle f_{12}\rangle_2 = \frac{1}{4\pi}\int \mathrm{d}\boldsymbol{r}_2 \int_{-1}^{1} \mathrm{d}\cos\theta_2 \int_0^{2\pi} \mathrm{d}\phi_2\ f_{12}. \tag{23}$$

The approximation is that the pair correlation function between particles 1 and 2 – which determines the total interaction energy – is written $g_{12} = W(\theta_1,t)W^\mathrm{id}(\theta_2,t)\Theta(r_{12}-\sigma)$, leading to the factorization apparent in Eqs. (11) and (22). Inserting Eq. (15) gives for the potential-energy function in the Fokker-Planck equation

$$\frac{U}{k_\mathrm{B}T} = -\left[\alpha_z + \chi_\mathrm{L}L(\alpha_z) + \alpha e^{i\omega t}\left(1+\frac{1}{3}\chi_\mathrm{L}Z_1^\mathrm{id}\right)\right]\cos\theta \tag{24}$$

where the label '1' is now omitted. As before, assuming that the probing ac field is small ($\alpha \ll 1$), the solution of Eq. (11) can be written as

$$W(\theta,t) = \left(\frac{\bar{\alpha}_z}{\sinh\bar{\alpha}_z}\right)e^{\bar{\alpha}_z\cos\theta} + \alpha e^{i\omega t}\sum_{n=0}^{\infty} Z_n P_n(\cos\theta) \tag{25}$$

where

$$\bar{\alpha}_z = \alpha_z + \chi_\mathrm{L}L(\alpha_z) \tag{26}$$

is an effective static Langevin parameter. The first term on the rhs is the unnormalized equilibrium Boltzmann distribution at the MMF1 level [23]. Following the same procedure as in Section II B 1, the linearized solution of Eq. (11) leads to the following recurrence relation between the new coefficients Z_n:

$$\begin{aligned} -Z_{n-1}\left[\frac{\bar{\alpha}_z n(n+1)}{2n-1}\right] + Z_n\left[n(n+1)+2i\omega\tau_\mathrm{B}\right] + Z_{n+1}\left[\frac{\bar{\alpha}_z n(n+1)}{2n+3}\right] \\ = -\left(\frac{2n+1}{2}\right)F_n(\bar{\alpha}_z)\left(1+\frac{1}{3}\chi_\mathrm{L}Z_1^\mathrm{id}\right). \end{aligned} \tag{27}$$

As before, $Z_0 = 0$ and the sum in Eq. (25) is truncated at $n = 5$, with $Z_{n>5} = 0$. The solution of the five algebraic relations gives for the first coefficient

$$Z_1 = G(\bar{\alpha}_z, \omega\tau_\mathrm{B})\left(1+\frac{1}{3}\chi_\mathrm{L}Z_1^\mathrm{id}\right) \tag{28}$$

where both Z_1 and $Z_1^{\rm id}$ depend on the same function G, but with the effective and bare applied static fields, respectively. The magnetization and frequency-dependent susceptibility follow from similar equations to Eqs. (18) and (19), respectively, with the results

$$M_z(t) = \rho\mu L(\bar{\alpha}_z) + \chi_{\rm L} h e^{i\omega t} Z_1 \tag{29}$$

$$\chi_z(\omega) = \chi_{\rm L} Z_1. \tag{30}$$

In the zero-frequency limit ($\omega\tau_{\rm B} \to 0$), the magnetization curve and static susceptibility are given by

$$M_z = \rho\mu L(\bar{\alpha}_z) \tag{31}$$

$$\chi_z(0) = \chi_{\rm L} G(\bar{\alpha}_z, 0) \left[1 + \frac{1}{3}\chi_{\rm L} G(\alpha_z, 0)\right] \tag{32}$$

where $G(a,0)$ was defined in Eq. (21). In the limit $\alpha_z \to 0$, $G(0,0) = 1$, and the familiar MMF1 result for the initial susceptibility $\chi_{\rm L}(1 + \chi_{\rm L}/3)$ is recovered [23].

C. Dynamical properties: the frequency-dependent susceptibility perpendicular to a static magnetic field

The development closely mirrors that in Section II B. To emphasize this, the same symbols will be used here as far as possible, but of course the definitions will be different. The ferrofluid is contained in a long, cylindrical tube oriented along the y axis. The magnetic field applied to the ferrofluid is of the form

$$\boldsymbol{H} = (0, h e^{i\omega t}, H_z) \tag{33}$$

where the weak, time-dependent, probing field causes a small magnetization in the y direction, which will be used only to define the frequency-dependent susceptibility within the linear-response regime. Demagnetization fields in the y direction are absent, but those in the z direction must be taken into account when interactions between particles are included (Section II C 2). The orientation of each dipole is characterized by the polar angle θ and the azimuthal angle ϕ. The Fokker-Planck equation for the probability distribution function $W(\theta, \phi, t)$ is

$$\begin{aligned} 2\tau_{\rm B}\frac{\partial W}{\partial t} = {} & \frac{1}{\sin\theta}\frac{\partial}{\partial\theta}\left[\sin\theta\left(\frac{\partial W}{\partial\theta} + \frac{W}{k_{\rm B}T}\frac{\partial U}{\partial\theta}\right)\right] \\ & + \frac{1}{\sin^2\theta}\frac{\partial}{\partial\phi}\left(\frac{\partial W}{\partial\phi} + \frac{W}{k_{\rm B}T}\frac{\partial U}{\partial\phi}\right). \end{aligned} \tag{34}$$

In Refs. 29 and 30, the longest characteristic time controlling the dynamics of the magnetization perpendicular to the applied field was found to be

$$\tau_\perp = \left[\frac{2L(\alpha_z)}{\alpha_z - L(\alpha_z)}\right]\tau_{\rm B} \tag{35}$$

which in small fields reduces to $\tau_\perp = \left(1 - \frac{1}{10}\alpha_z^2\right)\tau_{\rm B}$. The imaginary part of the susceptibility spectrum would be expected to show a peak at a frequency $\Omega_\perp \simeq \tau_\perp^{-1}$, which increases with increasing field strength.

1. Non-interacting particles

In the ideal, non-interacting case, the potential energy of a dipole in units of $k_{\rm B}T$ is

$$\frac{U}{k_{\rm B}T} = -\alpha_z\cos\theta - \alpha e^{i\omega t}\sin\theta\sin\phi. \tag{36}$$

Equation (34) can be solved by expanding W in terms of a set of spherical harmonics, but since U is a function of $\sin\phi$, the expansion need only contain terms to that order. Treating $\alpha \ll 1$ as a small parameter, and linearizing Eq. (34) gives the solution

$$W^{\rm id}(\theta,\phi,t) = \left(\frac{\alpha_z}{\sinh\alpha_z}\right)e^{\alpha_z\cos\theta} + \alpha e^{i\omega t}\sum_{n=0}^{\infty} Z_n^{\rm id}P_n^1(\cos\theta)\sin\phi \tag{37}$$

where $P_n^1(\cos\theta) = \sin\theta\,[{\rm d}P_n(\cos\theta)/{\rm d}\cos\theta]$ are associated Legendre polynomials. Equation (37) yields the following recurrence relation for the coefficients $Z_n^{\rm id}$, with $Z_0^{\rm id} = 0$.

$$\begin{aligned} Z_{n-1}^{\rm id}\left[\frac{\alpha_z(n-1)(n+1)}{2n-1}\right] - Z_n^{\rm id}\left[n(n+1) + 2i\omega\tau_{\rm B}\right] - Z_{n+1}^{\rm id}\left[\frac{\alpha_z n(n+2)}{2n+3}\right] \\ = -\left(\frac{2n+1}{2}\right)\frac{(n-1)!}{(n+1)!}F_n(\alpha_z) \end{aligned} \tag{38}$$

The coefficients $Z_n^{\rm id}$ depend on both α_z and ω, and the functions F_n are given by

$$F_n(a) = \left(\frac{a}{\sinh a}\right)\int_{-1}^{1} P_n^1(x)\left[\frac{e^{ax}}{\sqrt{1-x^2}} + \frac{\rm d}{{\rm d}x}\left(e^{ax}x\sqrt{1-x^2}\right)\right]{\rm d}x. \tag{39}$$

Once $W^{\rm id}$ is determined, the magnetization in the y direction is given by

$$\begin{aligned} M_y^{\rm id}(t) &= \frac{1}{4\pi}\rho\mu\int_0^{\pi}\int_0^{2\pi} W^{\rm id}(\theta,\phi,t)\sin^2\theta{\rm d}\theta\sin\phi{\rm d}\phi \\ &= \frac{1}{4}\rho\mu\alpha e^{i\omega t}\sum_{n=1}^{\infty} Z_n^{\rm id}\int_{-1}^{1} P_n^1(x)\sqrt{1-x^2}\,{\rm d}x \\ &= \chi_{\rm L}he^{i\omega t}Z_1^{\rm id}. \end{aligned} \tag{40}$$

The frequency-dependent susceptibility in the y direction is

$$\chi_y^{\rm id}(\omega) = \frac{\partial M_y^{\rm id}}{\partial (h e^{i\omega t})} = \chi_L Z_1^{\rm id} \tag{41}$$

where $Z_1^{\rm id}$ depends on the higher coefficients through the recurrence relation in Eq. (38). Of course, the representation of $W^{\rm id}$ in Eq. (37) has to be truncated at some arbitrary order to give a closed set of algebraic equations, and as in Section II B, this is done at $n = 5$ with $Z_{n>5}^{\rm id} = 0$. The calculation is outlined in Appendix B, where $Z_1^{\rm id} = G(\alpha_z, \omega\tau_{\rm B})$ is written to emphasize the dependence of the susceptibility on α_z and ω. As before, the function G has the property that $G(0,0) = 1$. In the zero-frequency limit ($\omega\tau_{\rm B} \to 0$), the static susceptibility in the y direction is

$$\chi_y^{\rm id}(0) = \chi_{\rm L} G(\alpha_z, 0) \tag{42}$$

$$G(\alpha_z, 0) = -3\left[\frac{L(\alpha_z)(2659\alpha_z^4 + 154092\alpha_z^2 + 1188000) - 160\alpha_z(\alpha_z^4 + 189\alpha_z^2 + 3465)}{\alpha_z(701\alpha_z^4 + 47508\alpha_z^2 + 475200)}\right] \tag{43}$$

In Section III A, this approximate relation will be tested against the exact formula in Eq. (8). In the limit $\alpha_z \to 0$, $G(0,0) = 1$, and the Langevin initial susceptibility is recovered.

2. Interacting particles

Including interactions is slightly more complicated in this case, because the static external magnetic field and the probing ac field are perpendicular to one another, with the ac field parallel to the long axis of the cylindrical container and the y direction. Therefore, demagnetization fields must be taken into account when dealing with the static field in the z direction. If the Langevin parameter corresponding to the external applied field in the z direction is $\alpha_z^{\rm ext}$, then the effective internal Langevin parameter at the MMF1 level is

$$\bar{\alpha}_z = \alpha_z^{\rm ext} - \frac{1}{2}\chi_{\rm L} L(\alpha_z^{\rm ext}). \tag{44}$$

Hence, at the MMF1 level, the potential energy for a single dipole is

$$\frac{U}{k_{\rm B}T} = -\bar{\alpha}_z \cos\theta - \alpha e^{i\omega t} \sin\theta \sin\phi \left(1 + \frac{1}{3}\chi_{\rm L} Z_1^{\rm id}\right). \tag{45}$$

Combining Eqs. (34) and (45) and linearizing with respect to the small parameter α leads to the solution

$$W(\theta, \phi, t) = \left(\frac{\bar{\alpha}_z}{\sinh\bar{\alpha}_z}\right) e^{\bar{\alpha}_z \cos\theta} + \alpha e^{i\omega t} \sum_{n=0}^{\infty} Z_n P_n^1(\cos\theta) \sin\phi \tag{46}$$

where the first term on the rhs corresponds to the unnormalized equilibrium Boltzmann distribution at the MMF1 level, when the static field is perpendicular to the cylinder axis. The recurrence relation for the coefficients Z_n is now

$$Z_{n-1}\left[\frac{\bar{\alpha}_z(n-1)(n+1)}{2n-1}\right] - Z_n\left[n(n+1)+2i\omega\tau_{\rm B}\right] - Z_{n+1}\left[\frac{\bar{\alpha}_z n(n+2)}{2n+3}\right] = -\left(\frac{2n+1}{2}\right)\frac{(n-1)!}{(n+1)!}F_n(\bar{\alpha}_z)\left(1+\frac{1}{3}\chi_{\rm L}Z_1^{\rm id}\right). \tag{47}$$

These equations are solved by truncation at $n = 5$, with $Z_0 = 0$ and $Z_{n>5} = 0$. The first coefficient is

$$Z_1 = G(\bar{\alpha}_z, \omega\tau_{\rm B})\left(1+\frac{1}{3}\chi_{\rm L}Z_1^{\rm id}\right) \tag{48}$$

where the function G is defined in Appendix B, and has the property $G(0,0) = 1$. The magnetization and frequency-dependent susceptibility are obtained in a similar fashion to the non-interacting results in Eqs. (40) and (41), respectively.

$$M_y(t) = \chi_{\rm L} h e^{i\omega t} Z_1 \tag{49}$$

$$\chi_y(\omega) = \chi_{\rm L} Z_1 \tag{50}$$

In the zero-frequency limit, the static susceptibility is given by

$$\chi_y(0) = \chi_{\rm L} G(\bar{\alpha}_z, 0)\left[1+\frac{1}{3}\chi_{\rm L}G(\alpha_z^{\rm ext}, 0)\right] \tag{51}$$

where $G(a,0)$ is written explicitly in Eq. (43). In the limit $\alpha_z^{\rm ext} \to 0$, $G(0,0) = 1$, and the familiar MMF1 initial susceptibility is recovered.

3. Demagnetization-field effects

The theoretical expressions will be compared with results from simulations carried out with conducting boundary conditions – see Section II D. In the simulations, the external static field and the internal static field are the same because there are no demagnetization effects, whereas in the theory, they are different because of the cylindrical shape of the sample. The simplest way to compare simulation and theory is to *ignore* all demagnetization fields in the theory. This is an artificial solution, but it is easier than carrying out the simulations in some specific geometry. To be clear, the comparison will be based on Eqs. (48), (50), and (51), but with α_z instead of $\alpha_z^{\rm ext}$, and $\bar{\alpha}_z$ given by Eq. (26) instead of Eq. (44); α_z

is the internal static Langevin parameter, as applied in simulations. But for comparing with experiments on long cylindrical samples, where demagnetization fields cannot be eliminated at will, Eq. (44) is the correct expression for $\bar{\alpha}_z$, defined in terms of the external static Langevin parameter $\alpha_z^{\rm ext}$. See Supplemental Material at [URL will be inserted by publisher] for a Mathcad worksheet for evaluating all of the necessary formulas [35].

D. Simulations

The theory is tested rigorously by comparison to BD simulations. The justification for this is that there are complicating factors associated with experimental measurements, including particle polydispersity, the contribution of Néel relaxation to the magnetic response [2, 4], and uncertainties concerning the thickness of the nonmagnetic layer, which can obscure the effects of dipole-dipole interactions on the Brownian-relaxation mechanism, and the concomitant changes to the frequency-dependent susceptibility. These effects are very difficult to isolate from experimental measurements, and so BD simulations offer a 'perfect' computational experiment with which to test the mathematical approximations made in the theory. Once it has been determined that the theory takes proper account of dipole-dipole interactions, then the additional factors can be included afterwards for comparison with experimental data.

BD simulations were carried out in the NVT ensemble by using Langevin dynamics with a Stokes-force friction coefficient that was high enough to suppress short-time inertial motion, while keeping the Brownian rotation time, and hence the simulation runs, as short as possible. The translational and rotational diffusion coefficients are $D_{\rm trans} = k_{\rm B}T/3\pi\eta\sigma$ and $D_{\rm rot} = k_{\rm B}T/\pi\eta\sigma^3$, respectively. Defining the Stokes-force friction coefficient as $\gamma = 3\pi\eta\sigma/m$, where m is the particle mass, gives $D_{\rm trans} = k_{\rm B}T/\gamma m$, $D_{\rm rot} = 3k_{\rm B}T/\gamma m\sigma^2$, and through (12) $\tau_{\rm B} = \gamma m\sigma^2/6k_{\rm B}T$. Simulations were carried out with LAMMPS [36, 37] using the velocity-Verlet algorithm, reduced time step $\delta t^* = 0.005$, and friction coefficient $\gamma^* = 20$ (the LAMMPS damping time is $\tau^*_{\rm damp} = 1/\gamma^*$), all in Lennard-Jones reduced units. The temperature was set to $T^* = 1$ in all cases, and so the Brownian rotation time was $\tau^*_{\rm B} = \gamma^*/6T^* = 10/3 = 667\delta t$. $N = 512$ dipolar WCA particles in a static uniform field were simulated in a cubic simulation cell of side L with periodic boundary conditions applied. The particle concentration is defined in Lennard-Jones units as $\rho^* = N\sigma^3/L^3$, and the

corresponding volume fraction is $\varphi = \pi\rho^*/6$. The long-range dipole-dipole interactions were computed using an Ewald sum with conducting boundary conditions; in this case, there are no demagnetization fields, and the internal and external applied magnetic fields are identical. All simulations consisted of 10^7 time steps after equilibration. The instantaneous magnetization vector was output every 5 time steps. The frequency-dependent susceptibility spectra were computed using the formula

$$\chi_\beta(\omega) = \chi_\beta(0)\left[1 + i\omega\int_0^\infty C_\beta(t)e^{i\omega t}\,\mathrm{d}t\right] \tag{52}$$

where $\beta = x, y, z$. The normalized magnetization autocorrelation functions (MACFs) are given by

$$C_\beta(t) = \frac{\langle \delta M_\beta(t)\delta M_\beta(0)\rangle}{\langle \delta M_\beta^2\rangle} \tag{53}$$

where $\delta M_\beta(t) = M_\beta(t) - \langle M_\beta\rangle$; $\langle M_z\rangle$ is the magnetization curve, while $\langle M_x\rangle = \langle M_y\rangle = 0$. The static susceptibilities are given by

$$\chi_\beta(0) = \frac{\mu_0\langle \delta M_\beta^2\rangle}{Vk_\mathrm{B}T}. \tag{54}$$

Results for $C_x(t)$ and $C_y(t)$, and $\chi_x(0)$ and $\chi_y(0)$, were averaged in order to calculate $\chi_{xy}(\omega)$. BD simulations were also carried out in exactly the same way as described above but without dipolar interactions, in order to compare with theoretical predictions for the non-interacting (ideal) case.

III. RESULTS

In all of the following, the susceptibility perpendicular to a static field applied along the z axis is referred to as χ_{xy}, reflecting the fact that in the BD simulations, the x and y components have been measured and averaged.

A. Static properties

Figure 1(a) and (b) shows the magnetization curve and static field-dependent susceptibilities of non-interacting particles as functions of the Langevin parameter α_z, from BD simulations and theory. The results are also reported in Table I. Figure 1(a) shows perfect agreement between the BD simulations and the Langevin theory (6). There are two

sets of theoretical lines in Fig. 1(b), one being the exact results from (8) and (9), and the other being the truncated expansions from Eqs. (20) and (42). Both sets of theoretical lines coincide with the simulation results in the range $\alpha_z \leq 5$. $\chi_{xy}^{\mathrm{id}}(0)$ and $\chi_z^{\mathrm{id}}(0)$ decrease with increasing field due to the energetic constraint of the dipolar orientation by the static applied field in the z direction, but obviously the effect is stronger in the field direction, and so $\chi_z^{\mathrm{id}}(0) < \chi_{xy}^{\mathrm{id}}(0)$. Equations (20) and (42) are only valid for $\alpha_z \lesssim 10$; they deviate from the exact results at higher values of α_z, as is shown explicitly in Fig. 1(c), but over the range $\alpha_z \leq 5$ studied in detail here, they are sufficient.

Figure 2 shows the magnetization curves of systems with $\lambda = 1.0$ and $\lambda = 2.5$, and at different concentrations $0.0 \leq \rho^* \leq 0.5$. With $\lambda = 1.0$, the BD simulation results and the MMF1 theory [Eq. (31)] are generally in good agreement, except at the highest concentration. With $\lambda = 2.5$, there are significant deviations at concentrations $\rho^* \geq 0.3$. These deviations are a result of growing positional and orientational correlations between the particles with increasing concentration [38], which are not captured precisely by the MMF1 approximation [Eq. (22)]. There are, of course, many higher-order theories that describe such correlations more accurately, such as the second-order modified mean-field theory [23, 39–44], integral equations [45, 46], various types of thermodynamic perturbation theories [47, 48], and cluster expansions [49, 50]. At present, the *dynamical* theory has not been extended beyond the MMF1 level, and so that is as far as this analysis is taken.

Figure 3 shows the static field-dependent susceptibilities of systems with $\lambda = 1.0$ and $\lambda = 2.5$, and concentrations $0.0 \leq \rho^* \leq 0.5$, as functions of the Langevin parameter α_z. The BD simulation results are given in Table II and III, while the theoretical results are from Eqs. (32) and (51). The plots show the ratios $\chi_\beta(0)/\chi_\beta^{\mathrm{id}}(0)$ to isolate the effects of interactions; it will be shown below that in all cases $\chi_z < \chi_{xy}$. The behavior is rather complex. In all cases, under low-field conditions, both $\chi_{xy}(0)/\chi_{xy}^{\mathrm{id}}(0)$ and $\chi_z(0)/\chi_z^{\mathrm{id}}(0)$ increase with increasing concentration due to the interparticle interactions; the increase is greater for the system with stronger dipolar interactions (λ). As the field is increased, $\chi_{xy}(0)$ decreases monotonically towards the ideal value, as the dipole-field interactions dominate over the dipole-dipole interactions and cause strong alignment of the dipoles in the z direction. With increasing field, $\chi_z(0)$ first decreases below the ideal value, and then increases again towards the ideal value, and under high-field conditions, it decreases with increasing concentration. This shows that there is an additional orientational constraint arising from the nose-to-tail dipolar

correlations which strongly reduces the susceptibility, and more so at high concentration. Overall, the agreement between MMF1 theory and simulation is very good.

An alternative visualization of the same results is given in Fig. 4, which shows the static field-dependent susceptibilities as functions of concentration ρ^*. The BD simulations show that $\chi_{xy}(0)/\chi_{xy}^{\mathrm{id}}(0)$ increases with increasing concentration, but that the slope decreases with increasing field strength, due to the dipole-field interactions becoming more important than the dipole-dipole interactions. The behavior of $\chi_z(0)/\chi_z^{\mathrm{id}}(0)$ is different: at low fields ($\alpha_z \leq 1$), $\chi_z(0) > \chi_z^{\mathrm{id}}(0)$ and increases with increasing concentration, while at higher fields, the opposite is true. Again, this reflects the cooperative effects of field and concentration on the chainlike correlations between particles. Overall, the MMF1 theory is generally reliable, as compared to BD simulations, for all values of λ and ρ^*.

B. Dynamic properties

The dynamical properties of non-interacting particles are characterized by the peak frequencies Ω^{id} in $\mathrm{Im}[\chi_{xy}^{\mathrm{id}}(\omega)]$ and $\mathrm{Im}[\chi_z^{\mathrm{id}}(\omega)]$. These are shown in Fig. 1(d), from both the theory and BD simulations. The predictions from the new, approximate theory were obtained by numerical differentiation of the imaginary part of the susceptibility spectrum. Both peak frequencies increase with increasing field strength due to the Zeeman force, which obviously affects the z (parallel) component of the magnetization directly and hence more strongly. As compared to the BD simulation results, Eqs. (13) and (35) are more accurate than the approximate theory; this is a direct consequence of the truncation of the probability distribution function $W(\theta, \phi, t)$ in the latter approach.

The susceptibility spectra for four systems with $\lambda = 1.0$ and 2.5, and $\rho^* = 0.1$ and 0.5, are shown in Figs. 5, 6, 7, and 8. The case of $\lambda = 1.0$ and $\rho^* = 0.1$ should be easiest to treat theoretically, because the effects of dipole-dipole interactions should be small. This is borne out by Fig. 5. At low to moderate frequencies (below the peaks in $\mathrm{Im}[\chi]$), both $\chi_{xy}(\omega)$ and $\chi_z(\omega)$ decrease with increasing field strength, and for a given frequency, $\chi_z(\omega) < \chi_{xy}(\omega)$; this is the same behavior as seen in the static susceptibilities in the non-interacting case discussed in Section III A. As the field strength is increased, the peaks in both $\chi_{xy}(\omega)$ and $\chi_z(\omega)$ shift to higher frequencies, again as seen in the non-interacting case. The agreement between theory and simulation is excellent for this case.

Figure 6 shows the susceptibility spectra for a system with $\lambda = 1.0$ and $\rho^* = 0.5$. Apart from the increase in χ_{xy} and χ_z, the changes in the spectra are subtle, and will be analyzed in more detail later. The main point, though, is that the MMF1 theory is less accurate at this higher concentration, although the static susceptibility is described accurately. The peak positions in $\mathrm{Im}[\chi_{xy}(\omega)]$ and $\mathrm{Im}[\chi_z(\omega)]$ are overestimated by the theory in low fields, and will be detailed below.

Figures 7 and 8 show the susceptibility spectra for systems with $\lambda = 2.5$, and $\rho^* = 0.1$ and 0.5, respectively. The key points here are that, in the BD simulations, the peak positions in the imaginary parts are shifted to much lower frequencies as compared to the $\lambda = 1.0$ case, and that the deviations between simulation and theory are substantial. The decreases in peak frequencies are signaling the onset of dipolar nose-to-tail correlations, and the concomitant increase in the characteristic rotation time. Although the theory gives fairly accurate predictions for all static susceptibilities with $\rho^* = 0.1$, there are noticeable discrepancies in χ_{xy} with $\rho^* = 0.5$, particularly with high values of α_z.

Figures 9 and 10 show how the peak positions Ω in the imaginary parts of the susceptibility spectra depend on α_z and ρ^*, respectively. The results are divided by the corresponding values in the non-interacting system in order to isolate the effects of dipole-dipole interactions. Recall from Fig. 1(d) that over the range $0 \leq \alpha_z \leq 5$, the peak frequencies $\Omega_{xy}^{\mathrm{id}}$ and Ω_z^{id} increase by factors of 2.6 and 4.0, respectively. The BD simulation results in Figure 9 show that, for a given concentration, $\Omega_{xy}/\Omega_{xy}^{\mathrm{id}}$ increases with increasing α_z towards 1. This is because the dipole-field interaction is increasing as compared to the dipole-dipole interaction. At low values of α_z, increasing the concentration leads to a decrease in $\Omega_{xy}/\Omega_{xy}^{\mathrm{id}}$, which is due to the transverse dipolar correlations and an increase in the characteristic rotation time. At high values of α_z, these transverse correlations are less significant as the dipoles are strongly aligned in the z direction, and so the concentration effect is reduced. The MMF1 theory captures most of these trends, but the agreement with simulation is only good with $\lambda = 1.0$ and $\rho^* \leq 0.2$. $\Omega_z/\Omega_z^{\mathrm{id}}$ shows different behavior, starting off below 1 at low field, and ending up above 1 at high field. At low field, the dipole-dipole correlations give a high characteristic rotation time and a low peak frequency; hence, increasing the concentration leads to a decrease in peak frequency. At high field, the dipole-field interactions cause strong alignment of the dipoles in the field direction, and this is enhanced by the interparticle interactions, particularly those in the nose-to-tail configuration; hence, increasing the concentration leads

to an increase in peak frequency. This behavior is captured qualitatively by the theory, but quantitative agreement with the BD simulations is lacking except with $\lambda = 1.0$ and $\rho^* \leq 0.2$. The theoretical predictions are inaccurate when all of λ, ρ^*, and α_z are large.

Figure 10 shows how the peak frequencies depend on concentration. The BD simulation results show that, in general, $\Omega_{xy}/\Omega_{xy}^{\mathrm{id}}$ decreases with increasing concentration, which is due to increasing dipole-dipole correlations and increasing characteristic rotation time. The magnitude of this effect is lower in stronger fields because there the dipole-field interactions are dominant. The theory is only reliable with low values of λ, ρ^*, and α_z. With increasing concentration, the BD simulations show that $\Omega_z/\Omega_z^{\mathrm{id}}$ decreases in low fields and increases in high fields, again reflecting the balance of dipole-dipole and dipole-field interactions. The theory is accurate only with the lowest values of λ, ρ^*, and α_z.

It emphasized that the results in Fig. 9 and 10 are presented in units of the peak frequency at zero concentration [Fig. 1(d)] in order to accentuate the dependence on dipolar interactions, but the absolute values of Ω_{xy} and Ω_z vary significantly with field strength, and hence plotting these absolute values would obscure the deviations between simulation and theory.

IV. CONCLUSIONS

In this work, the calculation of the magnetic susceptibility spectra of a ferrofluid in a static field was outlined. The presence of the static field introduces several technical complications as compared to the zero-field case: firstly, there are two susceptibility spectra, corresponding to the parallel and perpendicular orientations of the probing ac field with respect to the static field; secondly, the mathematical details of the problem necessitate an expansion with respect to the static-field Langevin parameter, as opposed to a simple closed-form expression; and thirdly, demagnetization-field effects have to be considered. Nonetheless, explicit expressions may be given for the susceptibility spectra, and these have been tested against numerical results from Brownian dynamics simulations. In the case of non-interacting magnetic nanoparticles (meaning, vanishing concentration) the theory and simulations are in good agreement, which justifies the initial choice of how many terms should be included in the expansion with respect to the static-field Langevin parameter. Interactions have been included at the first-order modified mean-field level, meaning that the susceptibility is ex-

panded in powers of $\rho\lambda$ up to second order; as a result, the theoretical results were expected to be accurate only at low concentration (ρ) and high temperature (λ^{-1}). Comparisons with simulations shows this to be the case. As long as $\rho\sigma^3 \sim 0.1$ and $\lambda \sim 1$, then the theory is reliable. Note that these parameters are typical for real ferrofluids at room temperature. As an example, a systematic analysis of the magnetization curves of magnetite ferrofluids with a very wide range of volume fractions $0.0303 \leq \varphi \leq 0.346$ [51] gave a consistent value of the average dipolar coupling constant at $T = 293$ K of $\lambda \simeq 0.965$ [41]. Ferrofluids with volume fractions $\varphi \gtrsim 0.2$ ($\rho^* \gtrsim 0.4$) are considered to be concentrated. A typical applied magnetic field of 100 kA m^{-1} corresponds to an average Langevin parameter of 4.74. These calculations are based on the assumption that the magnetization of the particle material is equal to its saturation value, justified *a posteriori* by the excellent agreement between theory and experiment. More recently, an ultracentrifugation analysis of magnetite-ferrofluid sedimentation profiles, and corresponding magnetization-curve measurements, gave dipolar coupling constants $\lambda \simeq 1$–2, depending on the particle size [52, 53]. The dynamical theory presented here is not intrinsically limited to this range of parameters; in principle, it can be extended by including interparticle interactions to higher order, and more straightforwardly, it can be extended to higher ranges of the static-field strength.

Overall, the effects of interparticle interactions are shown to be very significant. With increasing particle concentration, the static susceptibility parallel to a weak (strong) static field increases (decreases) by as much as a factor of 2–3, and the peak frequency in the imaginary part of the susceptibility decreases (increases) by tens of percent. This reflects the competition between interparticle interactions (which favor chain-like correlations, enhancing the susceptibility, and decreasing the peak frequency) and particle-field interactions (which cause strong alignment of the particles, decreasing the susceptibility, and increasing the peak frequency). With increasing particle concentration, the static susceptibility perpendicular to the applied static field increases, and the peak frequency decreases, but the changes are smaller with stronger static fields. This is due to particle-field interactions dominating interparticle interactions, causing the system to behave as in the non-interacting (zero-concentration) case.

ACKNOWLEDGMENTS

Support from Russian Science Foundation Grant No. 15-12-10003 is gratefully acknowledged. P.J.C. is grateful to Dr Julien Sindt (Edinburgh) for advice on setting up the Brownian dynamics simulations.

Appendix A: Expression for G in the parallel case

Solving the five algebraic equations yields the following result for the function $G(a,b)$.

$$G(a,b) = \frac{\tilde{D}(a,b)}{D(a,b)} \tag{A1}$$

$D(a,b)$ and $\tilde{D}(a,b)$ are determinants defined as follows.

$$D(a,b) = \begin{vmatrix} 2(1+ib) & \frac{2a}{5} & 0 & 0 & 0 \\ -2a & 2(3+ib) & \frac{6a}{7} & 0 & 0 \\ 0 & -\frac{12a}{5} & 2(6+ib) & \frac{4a}{3} & 0 \\ 0 & 0 & -\frac{20a}{7} & 2(10+ib) & \frac{20a}{11} \\ 0 & 0 & 0 & -\frac{10a}{3} & 2(15+ib) \end{vmatrix} \tag{A2}$$

$$\tilde{D}(a,b) = \begin{vmatrix} -\frac{3}{2}F_1(a) & \frac{2a}{5} & 0 & 0 & 0 \\ -\frac{5}{2}F_2(a) & 2(3+ib) & \frac{6a}{7} & 0 & 0 \\ -\frac{7}{2}F_3(a) & -\frac{12a}{5} & 2(6+ib) & \frac{4a}{3} & 0 \\ -\frac{9}{2}F_4(a) & 0 & -\frac{20a}{7} & 2(10+ib) & \frac{20a}{11} \\ -\frac{11}{2}F_5(a) & 0 & 0 & -\frac{10a}{3} & 2(15+ib) \end{vmatrix} \tag{A3}$$

The functions $F_n(a)$ are defined in Eq. (17). Explicit expressions for the first five functions are as follows.

$$F_1(a) = -\frac{4L(a)}{a} \tag{A4}$$

$$F_2(a) = -\frac{12L_3(a)}{a} \tag{A5}$$

$$F_3(a) = -24\left[\frac{L(a)}{a} - \frac{5L_3(a)}{a^2}\right] \tag{A6}$$

$$F_4(a) = 40\left[\frac{10L(a)}{a^2} - \frac{1}{a} - \frac{35L_3(a)}{a^3}\right] \tag{A7}$$

$$F_5(a) = 60\left[\frac{14}{a^2} - \frac{L(a)}{a} - \frac{105L(a)}{a^3} + \frac{315L_3(a)}{a^4}\right] \tag{A8}$$

$$L(a) = \coth a - \frac{1}{a} \tag{A9}$$

$$L_3(a) = 1 - \frac{3L(a)}{a} \tag{A10}$$

For the case $a = b = 0$, $F_1(0) = -\frac{4}{3}$, $F_{n>1}(0) = 0$, $D(0,0) = \tilde{D}(0,0) = 2 \times 6 \times 12 \times 20 \times 30$, and hence $G(0,0) = 1$.

Appendix B: Expression for G in the perpendicular case

Solving the five algebraic equations yields the following result for the function $G(a,b)$.

$$G(a,b) = \frac{\tilde{D}(a,b)}{D(a,b)} \tag{B1}$$

$D(a,b)$ and $\tilde{D}(a,b)$ are determinants defined as follows.

$$D(a,b) = \begin{vmatrix} -2(1+ib) & -\frac{3a}{5} & 0 & 0 & 0 \\ a & -2(3+ib) & -\frac{8a}{7} & 0 & 0 \\ 0 & \frac{8a}{5} & -2(6+ib) & -\frac{5a}{3} & 0 \\ 0 & 0 & \frac{15a}{7} & -2(10+ib) & -\frac{24a}{11} \\ 0 & 0 & 0 & \frac{8a}{3} & -2(15+ib) \end{vmatrix} \tag{B2}$$

$$\tilde{D}(a,b) = \begin{vmatrix} -\frac{3}{4}F_1(a) & -\frac{3a}{5} & 0 & 0 & 0 \\ -\frac{5}{12}F_2(a) & -2(3+ib) & -\frac{8a}{7} & 0 & 0 \\ -\frac{7}{24}F_3(a) & \frac{8a}{5} & -2(6+ib) & -\frac{5a}{3} & 0 \\ -\frac{9}{40}F_4(a) & 0 & \frac{15a}{7} & -2(10+ib) & -\frac{24a}{11} \\ -\frac{11}{60}F_5(a) & 0 & 0 & \frac{8a}{3} & -2(15+ib) \end{vmatrix} \tag{B3}$$

The functions $F_n(a)$ are defined in Eq. (39). Explicit expressions for the first five functions are as follows.

$$F_1(a) = 4\left[1 - \frac{L(a)}{a}\right] \tag{B4}$$

$$F_2(a) = 12\left[L(a) - \frac{2L_3(a)}{a}\right] \tag{B5}$$

$$F_3(a) = 24\left[1 - \frac{6L(a)}{a} + \frac{15L_3(a)}{a^2}\right] \tag{B6}$$

$$F_4(a) = 40\left[L(a) - \frac{9}{a} + \frac{55L(a)}{a^2} - \frac{140L_3(a)}{a^3}\right] \tag{B7}$$

$$F_5(a) = 60\left[1 - \frac{15L(a)}{a} - \frac{105}{a^2} + \frac{210L_3(a)}{a^2} + \frac{1575L_3(a)}{a^4}\right] \tag{B8}$$

For the case $a = b = 0$, $F_1(0) = \frac{8}{3}$, $F_{n>1}(0) = 0$, $D(0,0) = \tilde{D}(0,0) = (-2) \times (-6) \times (-12) \times (-20) \times (-30)$, and hence $G(0,0) = 1$.

[1] M. Shliomis, Usp. Fiz. Nauk **112**, 427 (1974).

[2] R. E. Rosensweig, *Ferrohydrodynamics* (Dover Publications, Inc., New York, 1998).

[3] P. J. Camp, in *Modern Problems of Molecular Physics*, Vol. Springer Proceedings in Physics 197, edited by L. Bulavin and A. Chalyi (Springer, New York, 2018) pp. 185–204.

[4] R. E. Rosensweig, J. Mag. Magn. Mater. **252**, 370 (2002).

[5] Q. A. Pankhurst, J. Connolly, S. K. Jones, and J. Dobson, J. Phys. D: Appl. Phys. **36**, R167 (2003).

[6] Q. A. Pankhurst, N. T. K. Thanh, S. K. Jones, and J. Dobson, J. Phys. D: Appl. Phys. **42**, 224001 (2009).

[7] R. Hergt, R. Hiergeist, I. Hilger, W. Kaiser, Y. Lapatnikov, S. Margel, and U. Richter, J. Magn. Magn. Mater. **270**, 345 (2004).

[8] F. Sonvico, S. Mornet, S. Vasseur, C. Dubernet, D. Jaillard, J. Degrouard, J. Hoebeke, E. Duguet, P. Colombo, and P. Couvreur, Bioconjug. Chem. **16**, 1181 (2005).

[9] J.-P. Fortin, C. Wilhelm, J. Servais, C. Ménager, J.-C. Bacri, and F. Gazeau, J. Am. Chem. Soc. **129**, 2628 (2007).

[10] R. Müller, R. Hergt, M. Zeisberger, and W. Gawalek, J. Mag. Magn. Mater. **289**, 13 (2005).

[11] Yu. L. Raikher and V. I. Stepanov, J. Mag. Magn. Mater. **368**, 421 (2014).

[12] M. Boskovic, G. F. Goya, S. Vranjes-Djuric, N. Jovic, B. Jancar, and B. Antic, J. Appl. Phys. **117**, 103903 (2015).

[13] W. F. Brown, Jr., J. Appl. Phys. **34**, 1319 (1963).

[14] W. F. Brown, Jr., IEEE Trans. Magn. **15**, 1196 (1979).

[15] P. Debye, *Polar Molecules* (Chemical Catalog Company, New York, 1929).

[16] H. Fröhlich, *Theory of dielectrics: dielectric constant and dielectric loss*, 2nd ed. (Clarendon Press, Oxford, 1987).

[17] A. Yu. Zubarev and A. V. Yushkov, J. Exp. Theor. Phys. **87**, 484 (1998).

[18] A. Yu. Zubarev and L. Yu. Isakova, Colloid J. **63**, 706 (2001).

[19] B. U. Felderhof and R. B. Jones, J. Phys.: Condens. Matter **15**, 4011 (2003).

[20] P. Ilg and S. Hess, Z. Naturforsch. **58a**, 589 (2003).

[21] D. V. Berkov, L. Yu. Iskakova, and A. Yu. Zubarev, Phys. Rev. E **79**, 021407 (2009).

[22] P. M. Déjardin and F. Ladieu, J. Chem. Phys. **140**, 034506 (2014).

[23] A. O. Ivanov and O. B. Kuznetsova, Phys. Rev. E **64**, 041405 (2001).

[24] A. O. Ivanov, V. S. Zverev, and S. S. Kantorovich, Soft Matter **12**, 3507 (2016).

[25] A. O. Ivanov and V. S. Zverev, Magnetohydrodynamics **52**, 43 (2016).

[26] J. O. Sindt, P. J. Camp, S. S. Kantorovich, E. A. Elfimova, and A. O. Ivanov, Phys. Rev. E **93**, 063117 (2016).

[27] A. O. Ivanov, S. S. Kantorovich, E. A. Elfimova, V. S. Zverev, J. O. Sindt, and P. J. Camp, J. Mag. Magn. Mater. **431**, 141 (2017).

[28] A. O. Ivanov, S. S. Kantorovich, V. S. Zverev, A. V. Lebedev, A. F. Pshenichnikov, and P. J. Camp, J. Mag. Magn. Mater. **459**, 252 (2018).

[29] M. A. Martsenyuk, Yu. L. Raikher, and M. I. Shliomis, Sov. Phys. JETP **38**, 413 (1974).

[30] M. I. Shliomis and Yu. L. Raikher, IEEE Trans. Magn. **16**, 237 (1980).

[31] A. F. Pshenichnikov and A. A. Fedorenko, J. Mag. Magn. Mater. **292**, 332 (2005).

[32] F. Ludwig, A. Guillaume, M. Schilling, N. Frickel, and A. M. Schmidt, J. Appl. Phys. **108**, 033918 (2010).

[33] J. Dieckhoff, D. Eberbeck, M. Schilling, and F. Ludwig, J. Appl. Phys. **119**, 043903 (2016).

[34] T. M. Batrudinov, A. V. Ambarov, E. A. Elfimova, V. S. Zverev, and A. O. Ivanov, J. Mag. Magn. Mater. **431**, 180 (2017).

[35] "PTC Mathcad," `www.ptc.com` (2018).

[36] "LAMMPS Molecular Dynamics Simulator," `http://lammps.sandia.gov` (1995).

[37] S. Plimpton, J. Comp. Phys. **117**, 1 (1995).

[38] E. A. Elfimova, A. O. Ivanov, and P. J. Camp, J. Chem. Phys. **136**, 194502 (2012).

[39] A. O. Ivanov and O. B. Kuznetsova, Colloid J. **63**, 60 (2001).

[40] A. O. Ivanov and O. B. Kuznetsova, Colloid J. **68**, 430 (2006).

[41] A. O. Ivanov, S. S. Kantorovich, E. N. Reznikov, C. Holm, A. F. Pshenichnikov, A. V. Lebedev, A. Chremos, and P. J. Camp, Phys. Rev. E **75**, 061405 (2007).

[42] A. O. Ivanov, S. S. Kantorovich, E. N. Reznikov, C. Holm, A. F. Pshenichnikov, A. V. Lebedev, A. Chremos, and P. J. Camp, Magnetohydrodynamics **43**, 393 (2007).

[43] P. J. Camp, E. A. Elfimova, and A. O. Ivanov, J. Phys.: Condens. Matter **26**, 456002 (2014).

[44] A. Yu. Solovyova, E. A. Elfimova, A. O. Ivanov, and P. J. Camp, Phys. Rev. E **96**, 052609 (2017).

[45] M. S. Wertheim, J. Chem. Phys. **55**, 4291 (1971).

[46] K. I. Morozov and A. V. Lebedev, J. Mag. Mag. Mater. **85**, 51 (1990).

[47] Yu. A. Buyevich and A. O. Ivanov, Physica A **190**, 276 (1992).

[48] A. O. Ivanov, Magnetohydrodynamics **28**, 353 (1992).

[49] B. Huke and M. Lücke, Phys. Rev. E **62**, 6875 (2000).

[50] B. Huke and M. Lücke, Phys. Rev. E **67**, 051403 (2003).

[51] A. F. Pshenichnikov, V. V. Mekhonoshin, and A. V. Lebedev, J. Mag. Magn. Mater. **161**, 94 (1996).

[52] B. Luigjes, D. M. E. Thies-Weesie, A. P. Philipse, and B. H. Erné, J. Phys.: Condens. Matter **24**, 245103 (2012).

[53] B. Luigjes, D. M. E. Thies-Weesie, B. H. Erné, and A. P. Philipse, J. Phys.: Condens. Matter **24**, 245104 (2012).

TABLE I. Results for non-interacting systems from theory and BD simulations. α_z is the Langevin parameter, $\chi^{\rm id}_{xy}(0)$ and $\chi^{\rm id}_z(0)$ are, respectively, the static field-dependent susceptibilities in the xy and z directions, $\Omega^{\rm id}_{xy}$ and $\Omega^{\rm id}_z$ are, respectively, the peak frequencies in the imaginary parts of the susceptibility spectra in the xy and z directions, and $\tau_{\rm B}$ is the Brownian rotation time (12).

	Theory				BD			
α_z	$\chi^{\rm id}_{xy}(0)/\chi_{\rm L}$	$\chi^{\rm id}_z(0)/\chi_{\rm L}$	$\Omega^{\rm id}_{xy}\tau_{\rm B}$	$\Omega^{\rm id}_z\tau_{\rm B}$	$\chi^{\rm id}_{xy}(0)/\chi_{\rm L}$	$\chi^{\rm id}_z(0)/\chi_{\rm L}$	$\Omega^{\rm id}_{xy}\tau_{\rm B}$	$\Omega^{\rm id}_z\tau_{\rm B}$
0	1.000	1.000	1.000	1.000	1.001(1)	1.001(1)	1.000(6)	1.001(3)
1	0.939	0.828	1.080	1.109	0.935(1)	0.819(1)	1.080(5)	1.124(5)
2	0.806	0.522	1.313	1.456	0.801(1)	0.522(1)	1.339(7)	1.48(1)
3	0.672	0.304	1.666	2.072	0.670(1)	0.300(1)	1.713(8)	2.12(2)
4	0.564	0.184	2.090	2.906	0.563(1)	0.181(1)	2.15(1)	2.99(2)
5	0.483	0.122	2.532	3.787	0.481(1)	0.118(1)	2.62(1)	3.99(3)

TABLE II. Results from BD simulations of ferrofluids with dipolar coupling constant $\lambda = 1.0$. ρ^* is the reduced concentration, $\chi_{\rm L}$ is the Langevin susceptibility (7), α_z is the Langevin parameter (4), $\chi_{xy}(0)$ and $\chi_z(0)$ are, respectively, the static field-dependent susceptibilities in the xy and z directions, Ω_{xy} and Ω_z are, respectively, the peak frequencies in the imaginary parts of the susceptibility spectra in the xy and z directions, and $\tau_{\rm B}$ is the Brownian rotation time (12).

ρ^*	$\chi_{\rm L}$	α_z	$\chi_{xy}(0)$	$\chi_z(0)$	$\Omega_{xy}\tau_{\rm B}$	$\Omega_z\tau_{\rm B}$
0.1	0.4189	0	0.4787(3)	0.4675(5)	0.831(6)	0.88(1)
		1	0.4416(3)	0.3617(4)	0.95(2)	1.02(2)
		2	0.3579(3)	0.2079(2)	1.25(1)	1.43(3)
		3	0.2962(2)	0.1153(1)	1.59(2)	2.15(5)
		4	0.2427(2)	0.0685(1)	2.06(3)	3.06(7)
		5	0.2061(1)	0.0448(0)	2.50(2)	4.21(8)
0.2	0.8378	0	1.0072(7)	1.018(1)	0.79(1)	0.79(1)
		1	0.9257(7)	0.7592(8)	0.89(1)	0.92(2)
		2	0.7484(5)	0.3988(4)	1.16(1)	1.46(3)
		3	0.6013(4)	0.2159(2)	1.53(2)	2.23(5)
		4	0.4926(3)	0.1294(1)	2.00(2)	3.21(6)
		5	0.4149(3)	0.0859(1)	2.46(3)	4.21(5)
0.3	1.2566	0	1.373(1)	1.352(1)	0.682(9)	0.72(1)
		1	1.537(1)	1.146(1)	0.80(1)	0.94(2)
		2	1.1856(8)	0.5651(6)	1.10(1)	1.43(3)
		3	0.9219(7)	0.2972(3)	1.55(2)	2.24(4)
		4	0.7503(5)	0.1761(2)	1.97(3)	3.36(7)
		5	0.6275(4)	0.1166(1)	2.47(3)	4.4(1)
0.4	1.6755	0	2.554(2)	2.619(3)	0.608(6)	0.601(5)
		1	2.183(2)	1.545(2)	0.76(1)	0.86(2)
		2	1.630(1)	0.6982(7)	1.10(1)	1.51(3)
		3	1.2654(9)	0.3609(4)	1.50(2)	2.48(5)
		4	1.0116(7)	0.2163(2)	2.00(3)	3.8(1)
		5	0.8458(6)	0.1449(1)	2.43(4)	4.8(2)
0.5	2.0944	0	3.559(3)	3.509(4)	0.541(5)	0.54(1)
		1	2.885(2)	1.952(2)	0.703(4)	0.86(1)
		2	2.110(2)	0.8323(8)	1.09(2)	1.51(3)
		3	1.596(1)	0.4165(4)	1.52(2)	2.62(4)
		4	1.2815(9)	0.2506(3)	1.97(3)	3.63(5)
		5	1.0658(8)	0.1674(2)	2.48(3)	4.86(8)

TABLE III. Results from BD simulations of ferrofluids with dipolar coupling constant $\lambda = 2.5$. ρ^* is the reduced concentration, $\chi_{\rm L}$ is the Langevin susceptibility (7), α_z is the Langevin parameter (4), $\chi_{xy}(0)$ and $\chi_z(0)$ are, respectively, the static field-dependent susceptibilities in the xy and z directions, Ω_{xy} and Ω_z are, respectively, the peak frequencies in the imaginary parts susceptibility spectra in the xy and z directions, and $\tau_{\rm B}$ is the Brownian rotation time (12).

ρ^*	$\chi_{\rm L}$	α_z	$\chi_{xy}(0)$	$\chi_z(0)$	$\Omega_{xy}\tau_{\rm B}$	$\Omega_z\tau_{\rm B}$
0.1	1.0472	0	1.393(1)	1.394(1)	0.54(1)	0.52(2)
		1	1.2524(9)	0.988(1)	0.62(2)	0.71(3)
		2	0.9581(7)	0.479(2)	0.85(2)	1.19(4)
		3	0.7541(5)	0.264(2)	1.22(3)	2.04(9)
		4	0.6215(4)	0.167(2)	1.44(4)	2.82(6)
		5	0.5217(4)	0.115(2)	1.94(6)	4.0(1)
0.2	2.0944	0	3.668(3)	3.628(4)	0.402(2)	0.362(7)
		1	2.936(2)	1.897(2)	0.47(1)	0.58(2)
		2	2.112(2)	0.7821(8)	0.72(1)	1.25(4)
		3	1.590(1)	0.4058(4)	1.07(3)	2.00(7)
		4	1.2959(9)	0.2443(2)	1.33(4)	3.2(1)
		5	1.0618(8)	0.1660(2)	1.78(6)	4.4(2)
0.3	3.1416	0	6.653(5)	6.375(6)	0.36(1)	0.325(6)
		1	4.945(3)	2.774(3)	0.47(1)	0.64(1)
		2	3.316(2)	1.047(1)	0.74(3)	1.27(3)
		3	2.473(2)	0.5265(5)	1.06(2)	2.28(9)
		4	1.958(1)	0.3245(3)	1.46(4)	3.5(1)
		5	1.625(1)	0.2203(2)	1.81(5)	4.8(2)
0.4	4.1888	0	10.113(7)	10.36(1)	0.299(3)	0.298(8)
		1	7.036(5)	3.523(4)	0.472(9)	0.62(2)
		2	4.597(3)	1.217(1)	0.76(2)	1.47(5)
		3	3.377(2)	0.6211(6)	1.12(1)	2.5(1)
		4	2.650(2)	0.3864(4)	1.50(5)	3.9(2)
		5	2.180(2)	0.2655(3)	1.88(5)	4.91(3)
0.5	5.2360	0	15.00(1)	14.51(1)	0.248(4)	0.25(2)
		1	9.407(7)	4.136(4)	0.443(9)	0.66(1)
		2	5.913(4)	1.365(1)	0.79(1)	1.6(1)
		3	4.319(3)	0.7043(7)	1.17(3)	2.6(1)
		4	3.340(2)	0.4364(4)	1.59(3)	3.9(2)
		5	2.753(2)	0.3023(3)	2.03(7)	4.8(4)

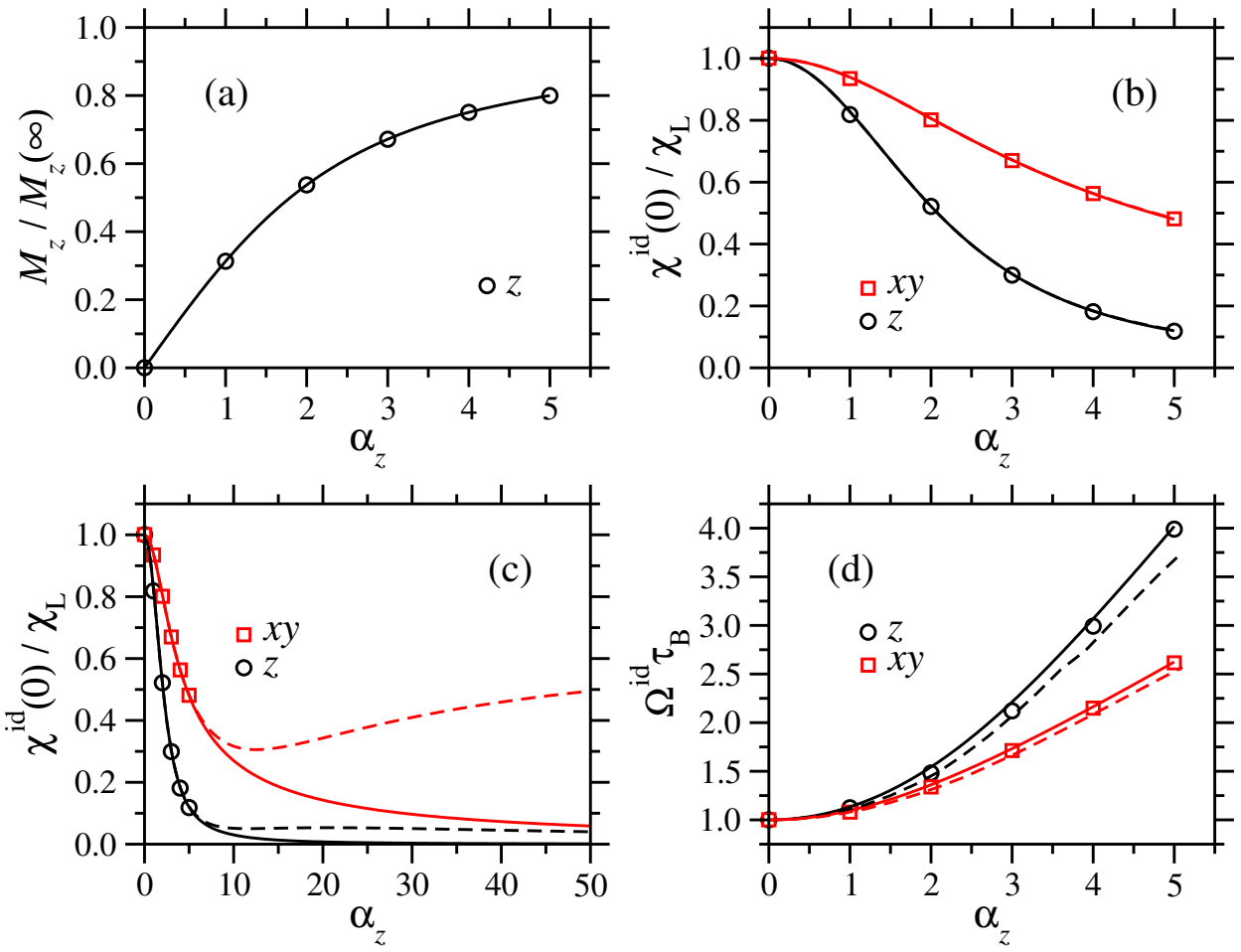

FIG. 1. Field-dependent properties of the one-particle model describing an ideal superparamagnetic gas with Langevin parameter α_z. (a) $M_z/M_z(\infty)$ is the fractional magnetization in the z direction. The solid line is the exact result [Eq. (6)] and the points are from BD simulations. (b) and (c) $\chi^{\rm id}_{xy}(0)$ and $\chi^{\rm id}_z(0)$ are the field-dependent static susceptibilities in the xy and z directions, respectively. The solid lines are the exact results [Eqs. (8) and (9)], the dashed lines are the approximate results [Eqs. (20) and (42)], and the points are from BD simulations. In (b), the exact and approximate results are indistinguishable on the scale of the graph. (d) $\Omega^{\rm id}_{xy}$ and $\Omega^{\rm id}_z$ are the peak frequencies in the imaginary parts of the susceptibility spectra in the xy and z directions, respectively. $\tau_{\rm B}$ is the Brownian rotation time (12). The solid lines are $\Omega_\parallel\tau_{\rm B} = \tau_{\rm B}/\tau_\parallel$ and $\Omega_\perp\tau_{\rm B} = \tau_{\rm B}/\tau_\perp$ from Eqs. (13) and (35), respectively, the dashed lines are the approximate results [by numerical differentiation of Eqs. (19) and (41)], and the points are from BD simulations.

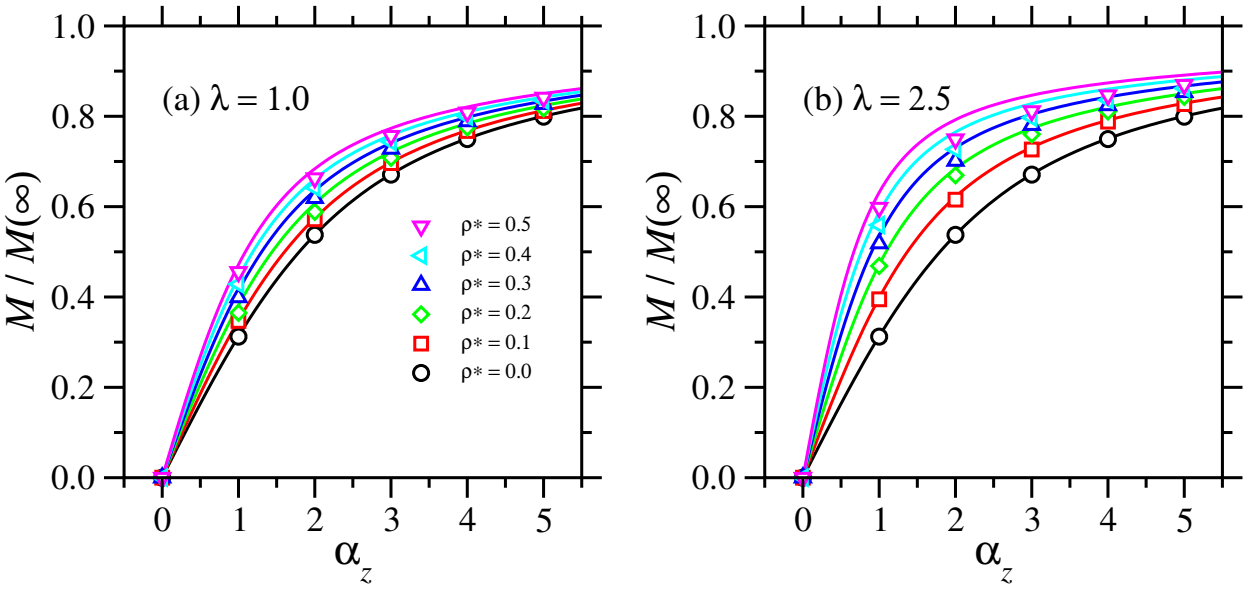

FIG. 2. Magnetization curves for ferrofluids with $\lambda = 1.0$ (a) and $\lambda = 2.5$ (b), and with concentrations $0.0 \leq \rho^* \leq 0.5$. The lines are from MMF1 theory (31) and the points are from BD simulations.

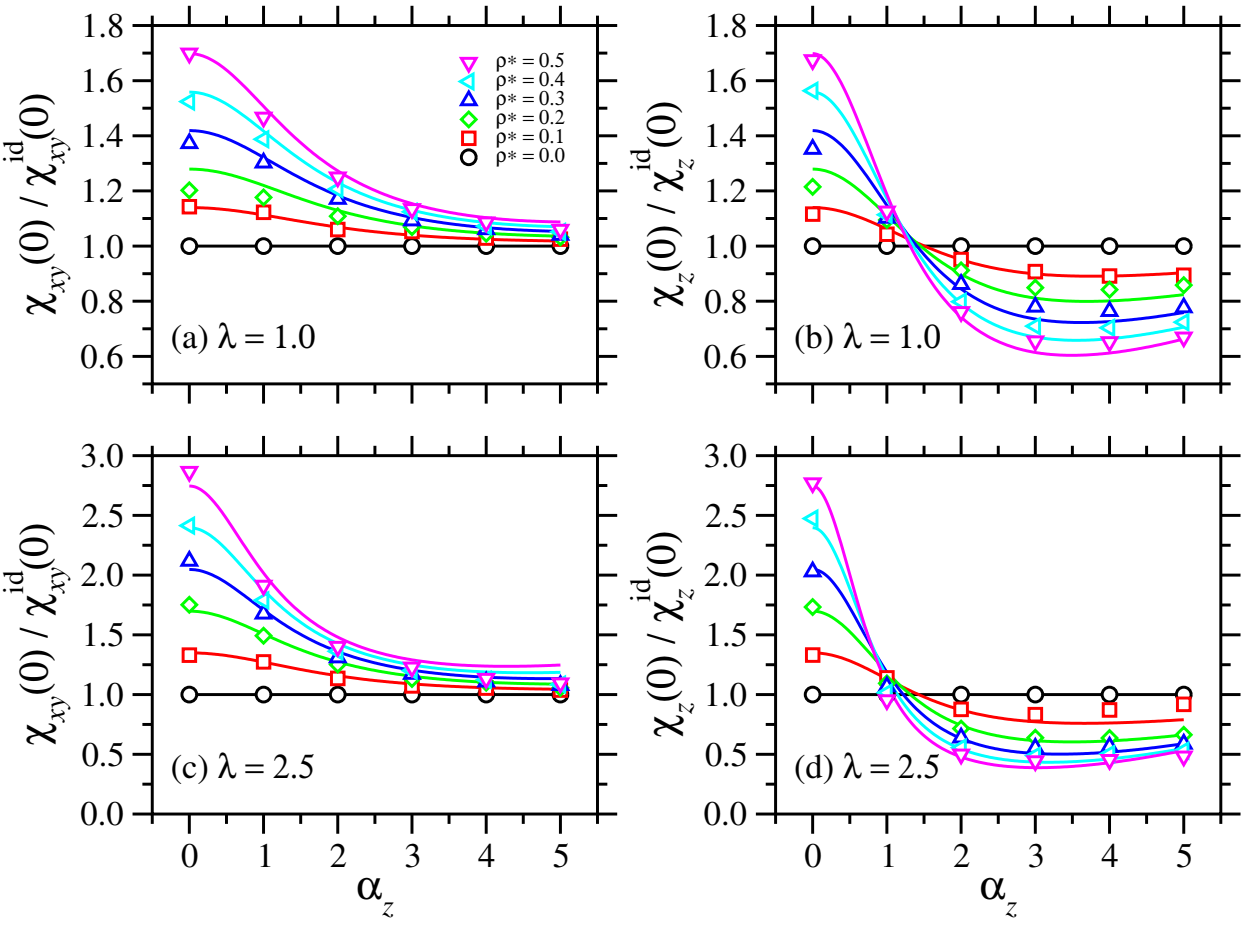

FIG. 3. Static field-dependent susceptibilities of ferrofluids with $\lambda = 1.0$ [(a) and (b)] and $\lambda = 2.5$ [(c) and (d)], and with concentrations $0.0 \leq \rho^* \leq 0.5$: (a) and (c) $\chi_{xy}(0)$; (b) and (d) $\chi_z(0)$. The results are shown divided by the respective ideal-gas susceptibilities $\chi_{xy}^{\rm id}(0)$ and $\chi_z^{\rm id}(0)$. The lines are from theory [(32), (51)] and the points are from BD simulations.

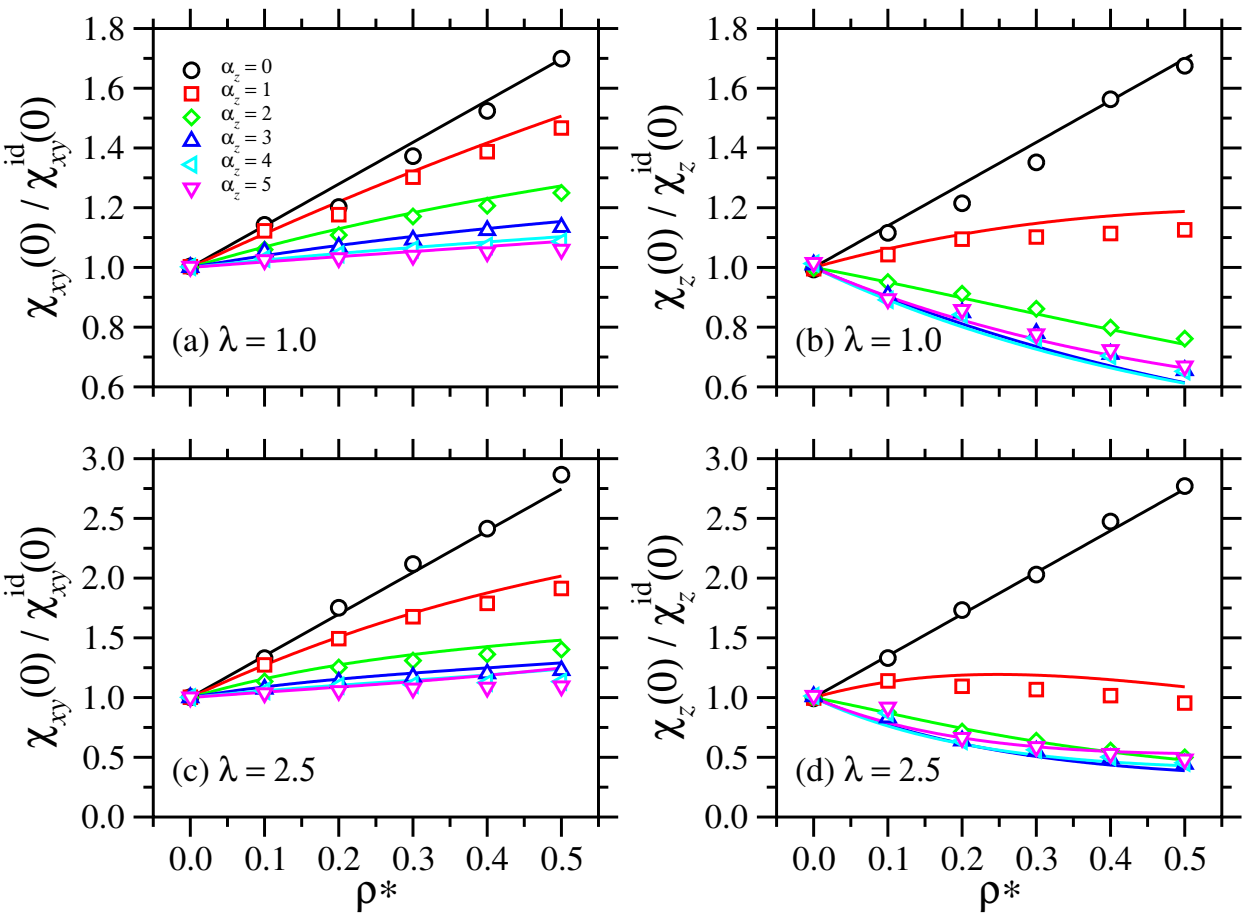

FIG. 4. Static concentration-dependent susceptibilities of ferrofluids with $\lambda = 1.0$ [(a) and (b)] and $\lambda = 2.5$ [(c) and (d)], and with Langevin parameters $0 \leq \alpha_z \leq 5$: (a) and (c) $\chi_{xy}(0)$; (b) and (d) $\chi_z(0)$. The results are shown divided by the respective ideal-gas susceptibilities $\chi^{\rm id}_{xy}(0)$ and $\chi^{\rm id}_z(0)$. The lines are from theory [(32), (51)] and the points are from BD simulations.

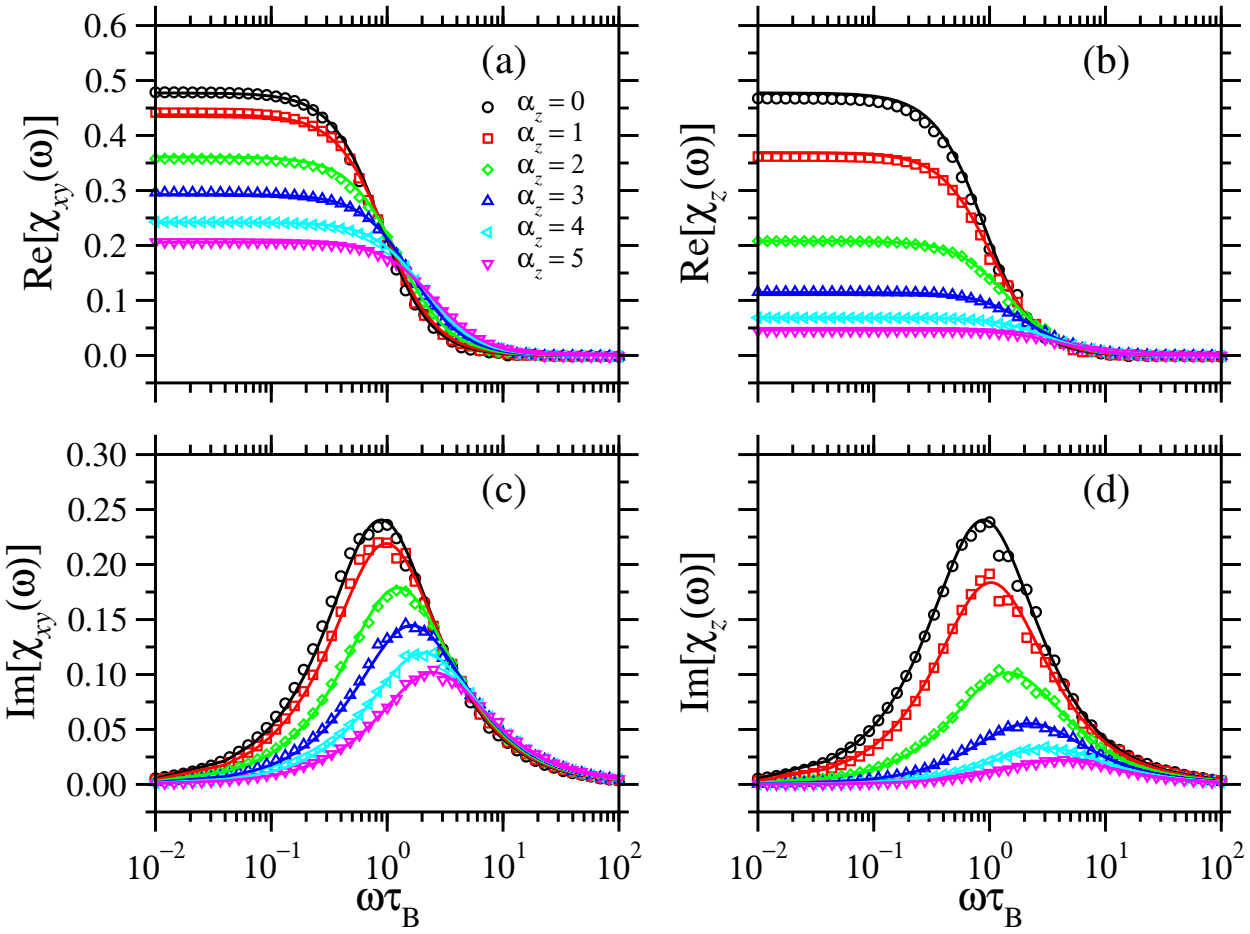

FIG. 5. Frequency-dependent susceptibilities of a ferrofluid with $\lambda = 1.0$ and $\rho^* = 0.1$. (a) and (b) show the real parts of $\chi_{xy}(\omega)$ and $\chi_z(\omega)$, respectively. (c) and (d) show the imaginary parts of $\chi_{xy}(\omega)$ and $\chi_z(\omega)$, respectively. The lines are from theory [(30), (50)] and the points are from BD simulations.

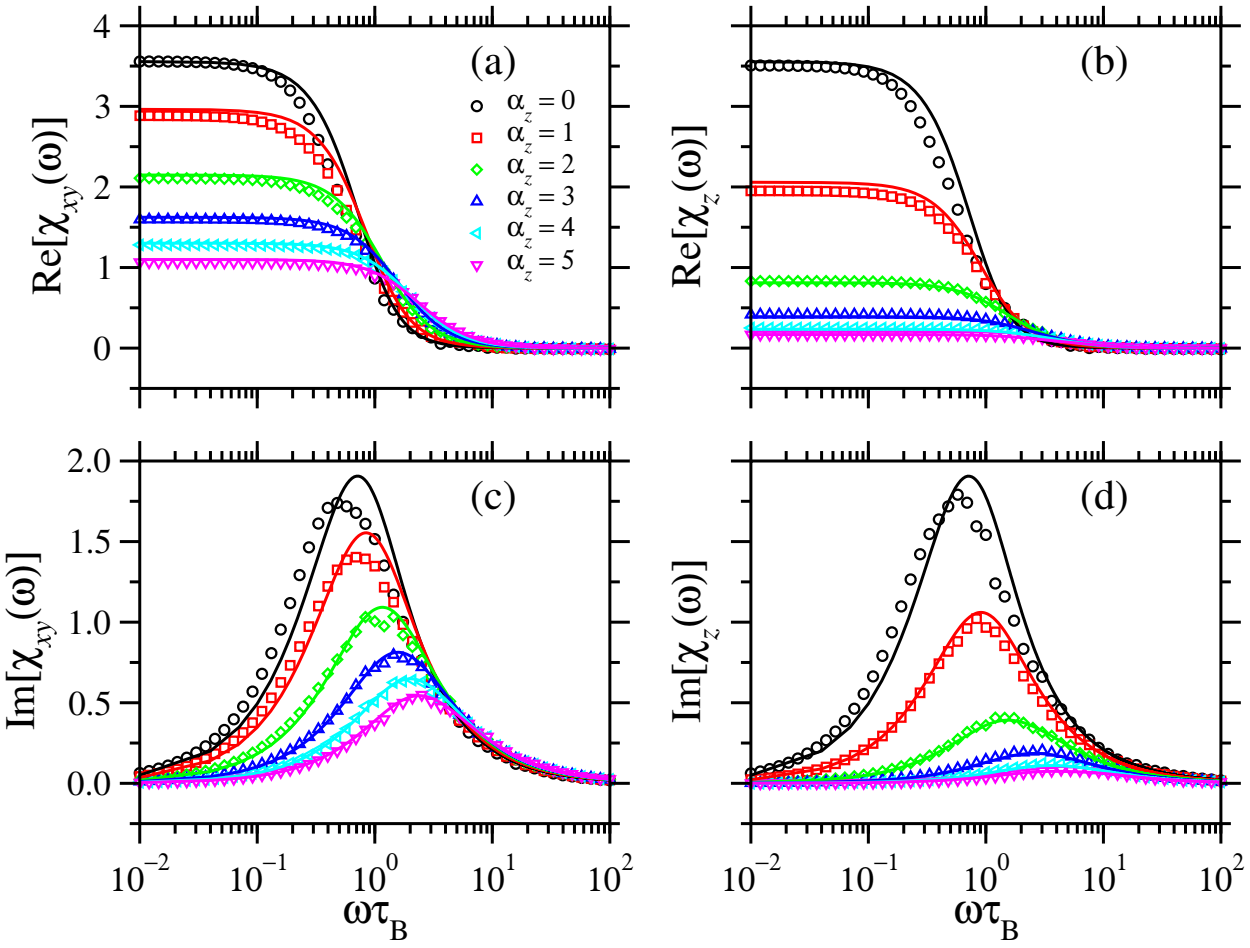

FIG. 6. Frequency-dependent susceptibilities of a ferrofluid with $\lambda = 1.0$ and $\rho^* = 0.5$. (a) and (b) show the real parts of $\chi_{xy}(\omega)$ and $\chi_z(\omega)$, respectively. (c) and (d) show the imaginary parts of $\chi_{xy}(\omega)$ and $\chi_z(\omega)$, respectively. The lines are from theory [(30), (50)] and the points are from BD simulations.

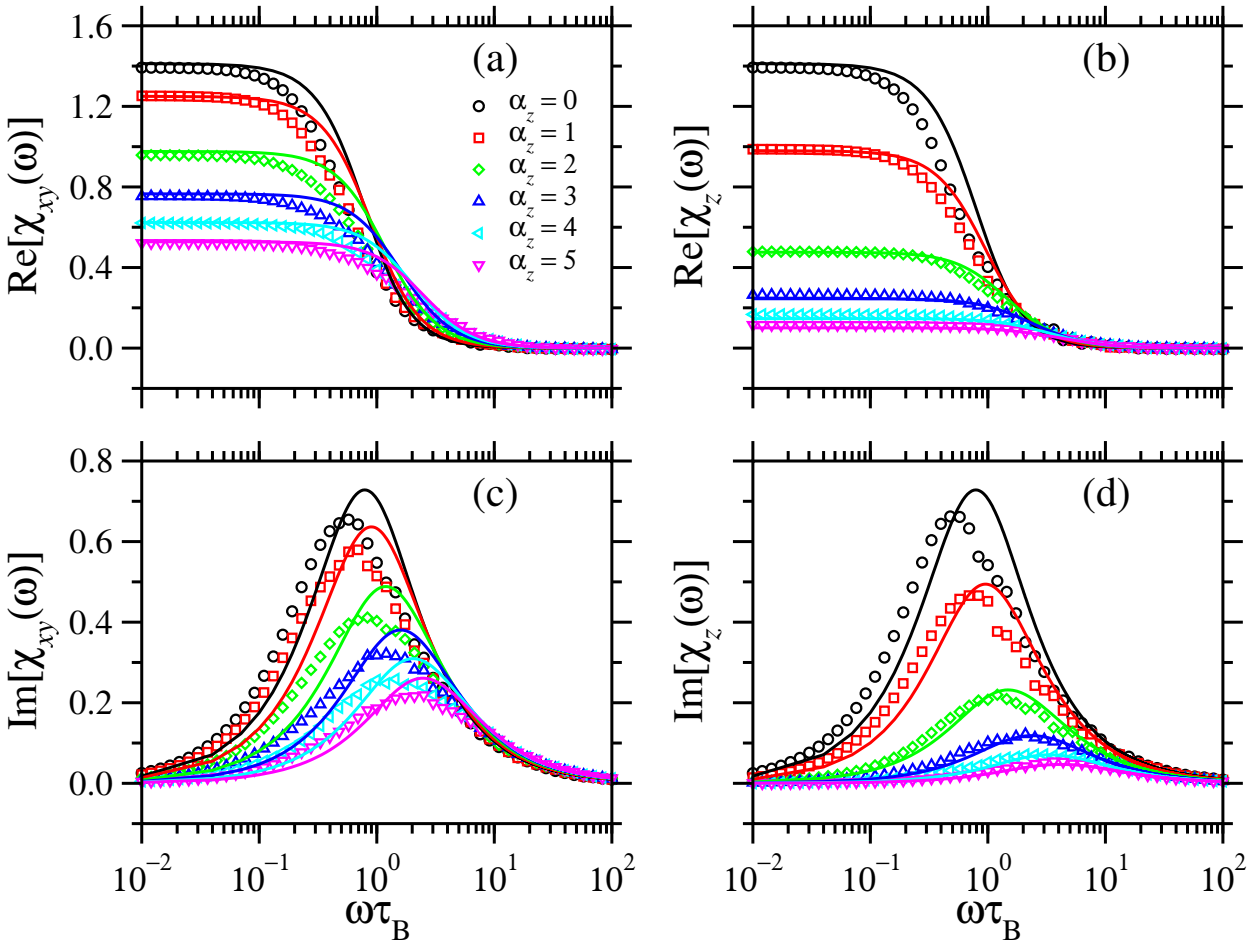

FIG. 7. Frequency-dependent susceptibilities of a ferrofluid with $\lambda = 2.5$ and $\rho^* = 0.1$. (a) and (b) show the real parts of $\chi_{xy}(\omega)$ and $\chi_z(\omega)$, respectively. (c) and (d) show the imaginary parts of $\chi_{xy}(\omega)$ and $\chi_z(\omega)$, respectively. The lines are from theory [(30), (50)] and the points are from BD simulations.

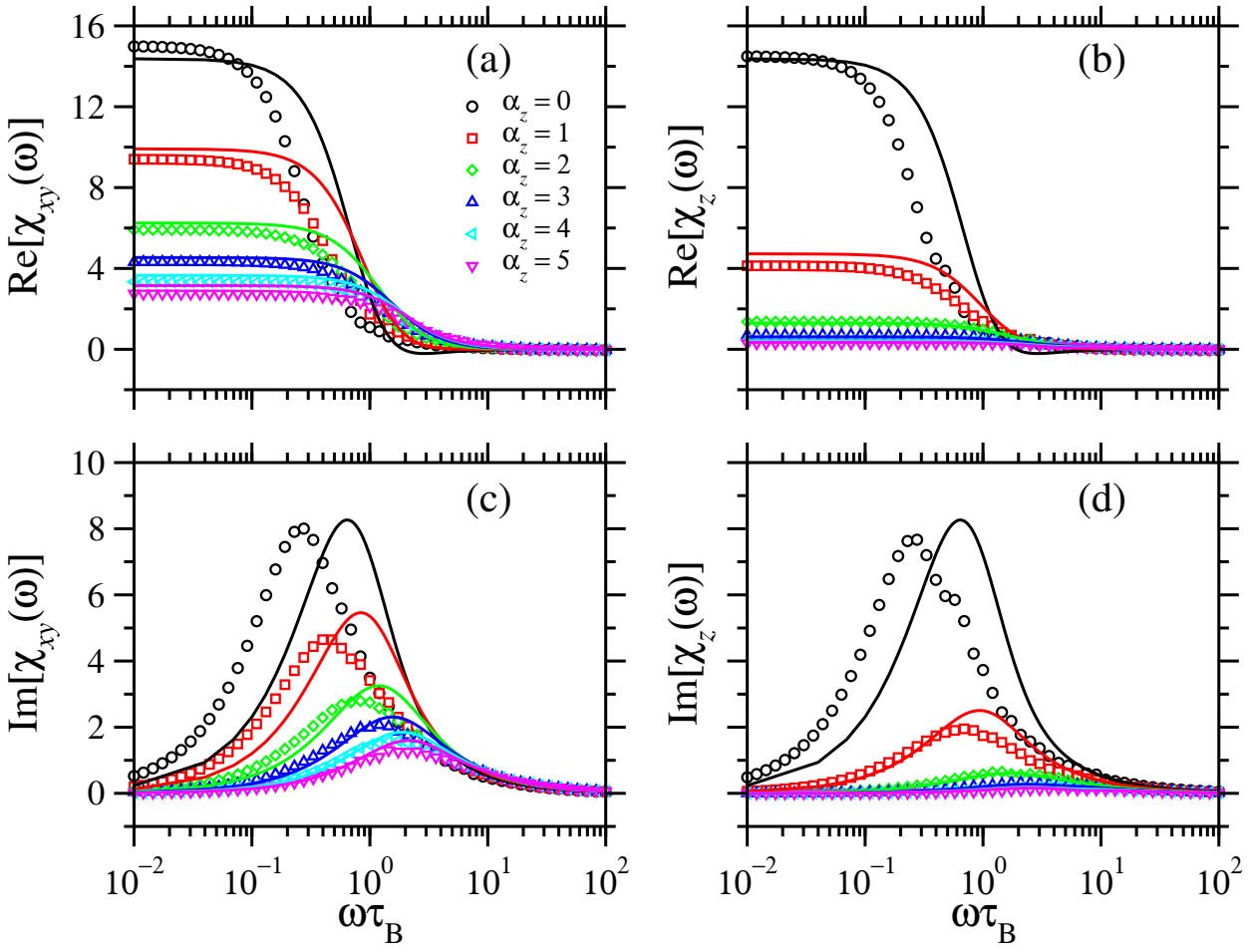

FIG. 8. Frequency-dependent susceptibilities for a ferrofluid with $\lambda = 2.5$ and $\rho^* = 0.5$. (a) and (b) show the real parts of $\chi_{xy}(\omega)$ and $\chi_z(\omega)$, respectively. (c) and (d) show the imaginary parts of $\chi_{xy}(\omega)$ and $\chi_z(\omega)$, respectively. The lines are from theory [(30), (50)] and the points are from BD simulations.

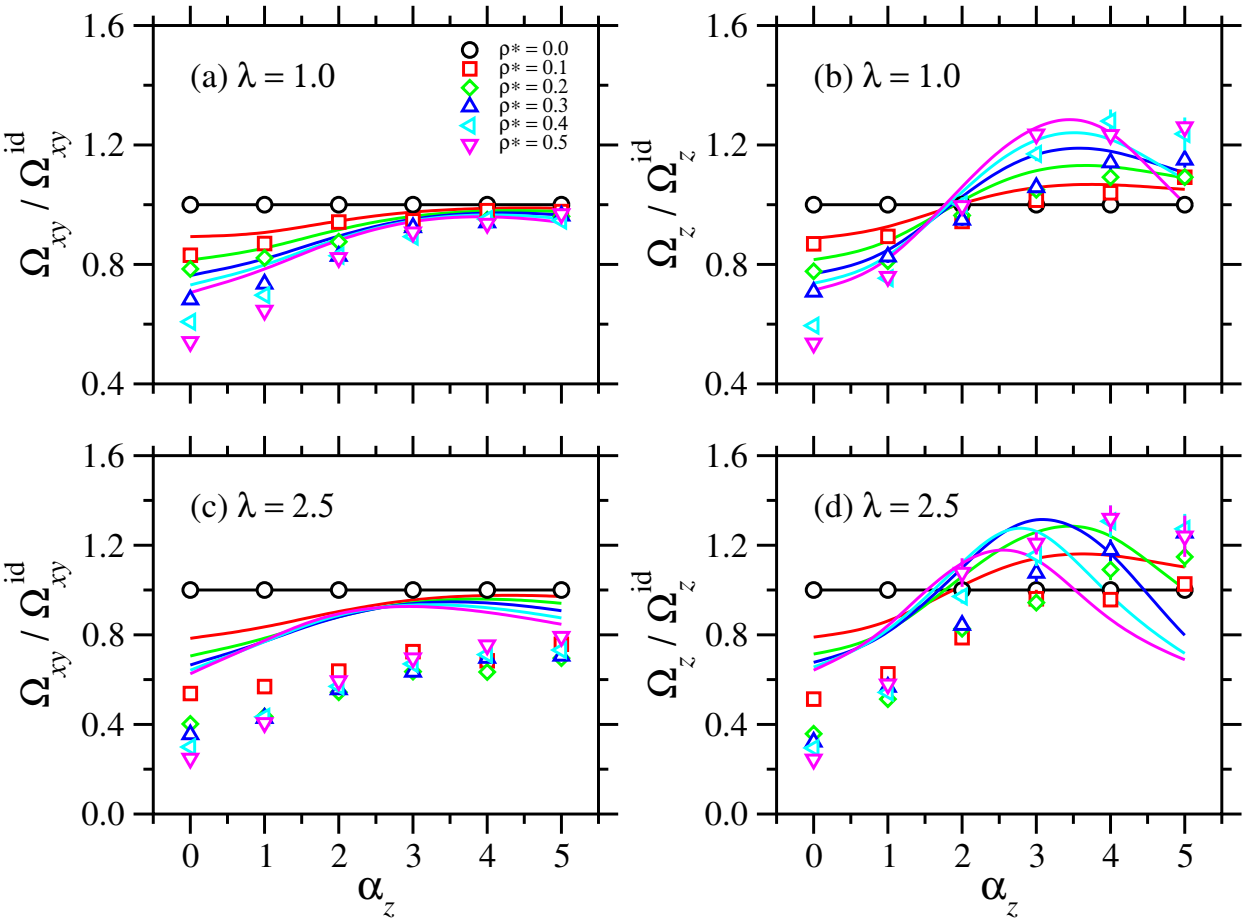

FIG. 9. Field-dependent peak frequencies of ferrofluids with $\lambda = 1.0$ [(a) and (b)] and $\lambda = 2.5$ [(c) and (d)], and with concentrations $0.0 \leq \rho^* \leq 0.5$: (a) and (c) Ω_{xy}; (b) and (d) Ω_z. The results are shown divided by the respective ideal-gas peak frequencies $\Omega_{xy}^{\mathrm{id}}$ and Ω_z^{id}. The lines are from theory and the points are from BD simulations.

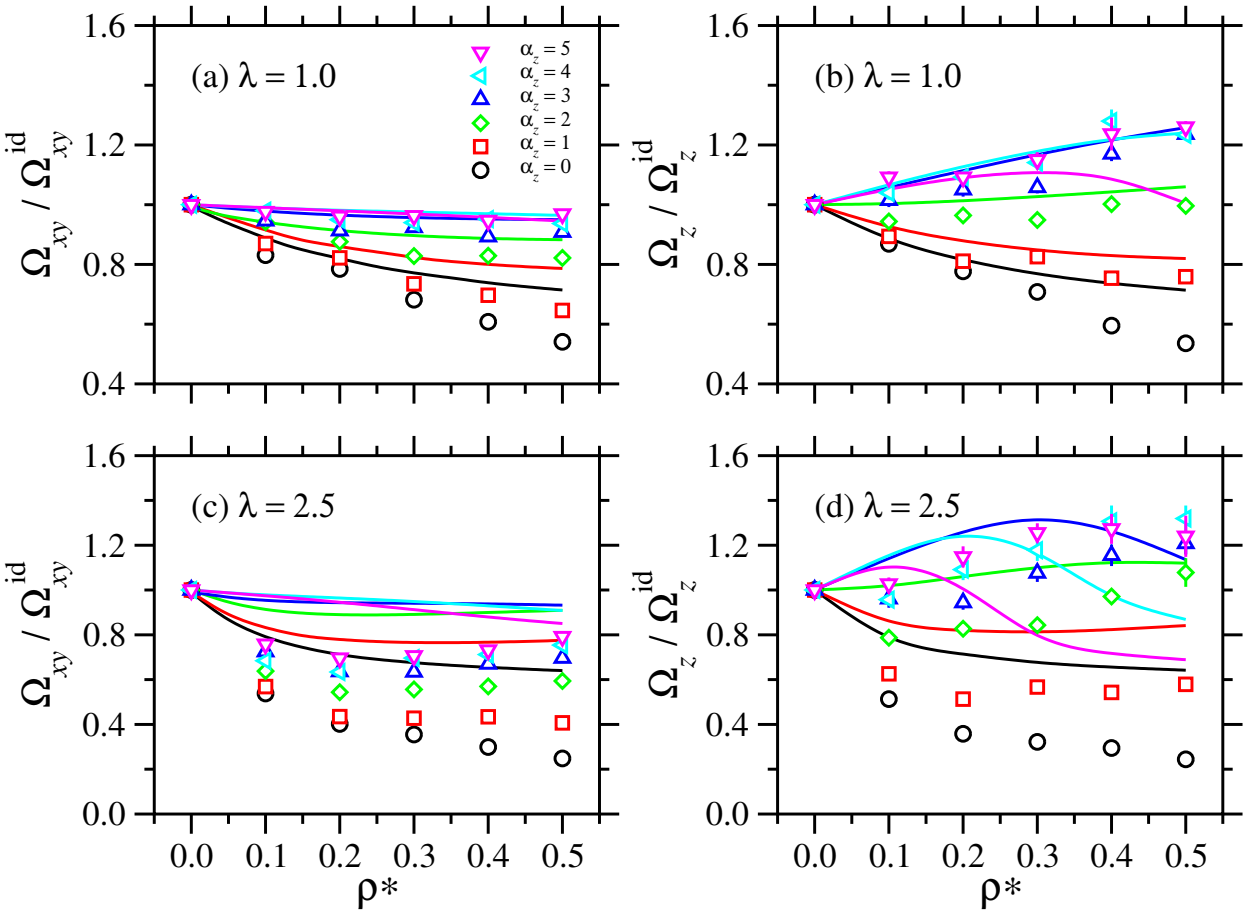

FIG. 10. Concentration-dependent peak frequencies of ferrofluids with $\lambda = 1.0$ [(a) and (b)] and $\lambda = 2.5$ [(c) and (d)], and with Langevin parameters $0 \leq \alpha_z \leq 5$: (a) and (c) Ω_{xy}; (b) and (d) Ω_z. The results are shown divided by the respective ideal-gas susceptibilities $\Omega_{xy}^{\rm id}$ and $\Omega_z^{\rm id}$. The lines are from theory and the points are from BD simulations.